Bioorg. Med. Chem. 77 (2023) 117111

Contents lists available at ScienceDirect

Bioorganic & Medicinal Chemistry

journal homepage: www.elsevier.com/locate/bmc

Exploration of 1,2,3-triazole linked benzenesulfonamide derivatives as isoform selective inhibitors of human carbonic anhydrase

Chnar Kakakhan [a], Cüneyt Türkeş [b,*], Özcan Güleç [a], Yeliz Demir [c], Mustafa Arslan [a,*], Gizem Özkemahlı [d], Şükrü Beydemir [e,f]

[a] Department of Chemistry, Faculty of Arts and Science, Sakarya University, 54187 Sakarya, Turkey
[b] Department of Biochemistry, Faculty of Pharmacy, Erzincan Binali Yıldırım University, 24002 Erzincan, Turkey
[c] Department of Pharmacy Services, Nihat Delibalta Göle Vocational High School, Ardahan University, 75700 Ardahan, Turkey
[d] Department of Toxicology, Faculty of Pharmacy, Erzincan Binali Yıldırım University, 24002 Erzincan, Turkey
[e] Department of Biochemistry, Faculty of Pharmacy, Anadolu University, 26470 Eskişehir, Turkey
[f] The Rectorate of Bilecik Şeyh Edebali University, 11230 Bilecik, Turkey

ARTICLE INFO

Keywords:
1,2,3-triazole
Benzenesulfonamide
Carbonic anhydrase
In silico study
Isoindoline

ABSTRACT

A novel series of 1,2,3-triazole benzenesulfonamide substituted 1,3-dioxoisoindolin-5-carboxylate (**7a-l**) inhibitors of human α-carbonic anhydrase (*h*CA) was designed using a tail approach. The design method relies on the hybridization of a benzenesulfonamide moiety with a tail of 1,3-dioxoisoindoline-5-carboxylate and a zinc-binding group on a 1,2,3-triazole scaffold. Among the synthesized analogues, 2-iodophenyl (**7f**, K_I of 105.00 nM and S_I of 2.98) and 2-naphthyl (**7h**, K_I of 32.11 nM and S_I of 3.48) analogues (over off-target *h*CA I) and phenyl (**7a**, K_I of 50.13 nM and S_I of 2.74) and 2,6-dimethylphenyl (**7d**, K_I of 50.60 nM and S_I of 3.35) analogues (over off-target *h*CA II) exhibited a remarkable selectivity for tumor isoforms *h*CA IX and XII, respectively. Meanwhile, analogue **7a** displayed a potent inhibitory effect against the tumor-associated isoform *h*CA IX (K_I of 18.29 nM) compared with the reference drug acetazolamide (AAZ, K_I of 437.20 nM), and analogue **7h** showed higher potency (K_I of 9.22 nM) than AAZ (K_I of 338.90 nM) against another tumor-associated isoform *h*CA XII. However, adding the lipophilic large naphthyl tail to the 1,3-dioxoisoindolin-5-carboxylate analogues increased both the *h*CA inhibitory and selective activities against the target isoform, *h*CA XII. Additionally, these analogues (**7a-l**) showed IC_{50} values against the human lung (A549) adenocarcinoma cancer cell line ranging from 129.71 to 352.26 μM. The results of the molecular docking study suggested that the sulfonamide moiety fits snugly into the *h*CAs active sites and interacts with the Zn^{2+} ion. At the same time, the tail extension engages in various hydrophilic and hydrophobic interactions with the nearby amino acids, which affects the potency and selectivity of the hybrids.

1. Introduction

Heterocyclic chemicals consisting of nitrogen are important components of many medicinal drugs, and biological molecules, including: vitamins, DNA, RNA, antigens, agrochemicals, and many others.[1–3] These compounds are also an important and characteristic category among applied organic chemistry and have a wide variety of physiological and pharmacological characteristics.[4–6] Triazoles can be classified into 1,2,3-triazole and 1,2,4-triazole because it has a five-membered ring of two carbon atoms and three nitrogen atoms.[7–9] It is simple to generate triazole, and the framework can function as an amide, ester, carboxylic acid, and other heterocycles like pyrazole isosteres.[10–12] One of the most significant classes of nitrogen-containing heterocycles, 1,2,3-triazoles, can generate a variety of non-covalent interactions with numerous biological targets,[13–15] including hydrophobic interactions, hydrogen bonds, van der Waals forces, and dipole–dipole

Abbreviations: AIC, akaike information criterion; AAZ, acetazolamide; DMF, dimethylformamide; DMSO, dimethylsulfoxide; DOX, doxorubicin; *h*CA, human α-carbonic anhydrase; *h*CAIs, *h*CA inhibitors; K_I, enzyme inhibition constants; R^2, K_I coefficient of determination; MM-GBSA, Molecular mechanics with generalized Born and surface area solvation; OPLS, optimal potential liquid simulations; SARs, structure-activity relationships; S_I, selectivity index; TBAB, tetrabutylammonium bromide.

* Corresponding authors.
E-mail addresses: cuneyt.turkes@erzincan.edu.tr (C. Türkeş), marslan@sakarya.edu.tr (M. Arslan).

https://doi.org/10.1016/j.bmc.2022.117111
Received 26 October 2022; Received in revised form 13 November 2022; Accepted 25 November 2022
Available online 29 November 2022

bonds. In medical chemistry, 1,2,3-triazole is considered a hetrocyclic 1,4-unsubstituted 1,2,3- triazole derivative, and can be synthesized via 1,3-dipolar reactions.[16–18] 1,3-Dipolar cycloaddition reactions are regarded as a powerful synthetic tool in constructing heterocyclic cycles, with uses in various fields.[19] Various pharmacological features of triazole compounds include antibacterial,[20] anti-tubercular,[21] anti-cancer,[22] and anti-malarial activity.[23] Several triazole-based medications, including Carboxyamidotriazole, Cefatrizine, Fluconazole, Rassinazole, and Ribavirin, have also been used in clinics or are now being tested in humans for the treatment of a variety of disorders.[24–26] As a result, triazole derivatives have an intriguing role to play in the creation of novel medications.

Fifteen different isoforms have been found in the human α-carbonic anhydrase (*h*CA, EC 4.2.1.1); all but *h*CA VIII, X, and XI are catalytically active.[27–28] This is because these isoforms lack the necessary histidine residues engaged in the catalytic process by coordinating the zinc-ion.[29–31] The twelve catalytically active *h*CAs have different tissue distribution and locations in the following places: For example, (i) *h*CA I, II, III, VII, and XIII are cytosolic; (ii) *h*CA IV, IX, XII, and XIV are membrane-associated; (iii) *h*CA VA and VB are mitochondrial; (iv) *h*CA VI is released in saliva and milk. It has been shown that inhibiting many of these *h*CA isoforms has significant druggable therapeutic effects for a variety of diseases, including edema (*h*CA II, IV, and XIV), glaucoma (*h*CA II, IV, and XII), central nervous system-associated pathologies (*h*CA VII and XIV), and malignancies (*h*CA IX and XII).[32–34] Discovering isoform-selective inhibitors is challenging since the active site design of these active α-*h*CAs is reasonably similar.[35] However, in these isoforms, the most variable amino acid residues are found at the active sites' entrances, while the most conserved ones are found at their bottom and middle regions.[36] *h*CA IX has been confirmed as a promising novel target in the discovery and development of anticancer drugs for managing hypoxic tumors due to its overexpression in various human malignancies.[37] The selectivity of *h*CA IX inhibitors over the physiologically significant cytosolic *h*CA I and II isoforms is a crucial factor to consider while designing them. Despite determining a number of methods for creating selective *h*CA IX inhibitors, the "tail approach" turned out to be the most successful and widely used.[38] In fact, it has been stated that this approach was taken into account in almost all drug design studies over the past ten years.[39] This method involves adding diverse chemical tails to an aromatic/heterocyclic ring with a zinc-binding group through a flexible linker, such as primary sulfamoyl and carboxylic acid functions (Scheme 1).

The current investigation is focused on employing the tail method to examine its impact on the potency and selectivity against the various *h*CA isoforms as a continuation of our efforts in the design and synthesis of new potent and selective *h*CA inhibitors (*h*CAIs). The designed 1,2,3-triazole benzenesulfonamide substituted 1,3-dioxoisoindolin-5-carboxylate analogues (**7a-l**) in this direction were synthesized, and various spectroscopic methods were used to determine their structural details (Scheme 2). Then, the inhibitory action of the target derivatives was then tested toward five different *h*CAs, including *h*CA I and II (off-target isoforms), IV (transmembrane isoform), IX, and XII (tumor-associated target isoforms). Additionally, an *in vitro* evaluation of the synthesized analogues' antiproliferative effects on the human lung adenocarcinoma cell line A549 was performed. Furthermore, molecular docking studies of the target analogues in these isoforms were conducted to study the expected *in silico* binding modes of the newly synthesized derivatives (**7a-l**) in the *h*CAs active sites.

2. Results and discussion

2.1. Drug design strategy and chemistry

Due to the substantial similarity among the active regions of *h*CAs, the tail approach emerged as one of the most promising strategies.[40] This method relies on adding differently designed aryl or heterocyclic

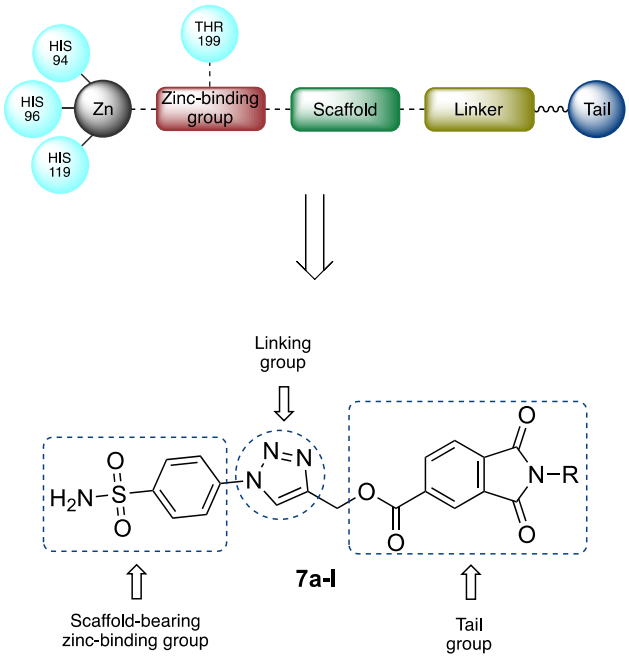

Scheme 1. Representation of "tail-approach" and the designed target 1,2,3-triazole based benzenesulfonamides **7a-l**.

scaffolds to the aromatic sulfonamide ring of the *h*CAIs in order to target specific hydrophobic/hydrophilic residues in the outer region of the isoform active site.[41] The target compounds (**7a-l**) in this formulation have a zinc-binding group of the benzenesulfonamide type that is attached to a triazole scaffold. This scaffold ensures that the tail of the compound is connected to the hydrophobic or hydrophilic rims of the active site in the proper orientation. Through advantageous interactions with the particular residues in the hydrophilic region of the active site, the 1,2,3-triazole moiety enhances the flexibility and hydrophilicity of the designed compounds to enforce selectivity towards *h*CA IX. The hydrophobic tail was also constructed using the 1,3-dioxoisoindoline-5-carboxylate moiety.

The compounds **3a-l** shown in Scheme 2 were prepared from a mixture of 1,3-dioxo-1,3-dihydroisobenzofuran-5-carboxylate and various amines in acetic acid by refluxing at 100 °C for 6 h. Then, **5a-l** compounds were synthesized from dissolving compound **3** in dimethylsulfoxide (DMSO) with K_2CO_3, TBAB, and propargyl bromide at room temperature for 6 h. The synthesis of triazole compounds with sulfonamide-bearing azide derivatives was prepared using $CuSO_4{\cdot}5H_2O$ and sodium ascorbate in DMF at 90 °C for 2 h. The structures of the targeted compounds (**7a-l**) were confirmed by the data ^{1}H NMR, ^{13}C NMR, FT-IR, and QTOF LC-MS analysis.

From the ^{1}H NMR data, the most characteristic peaks which are a singlet[1]H) at 8.15 ppm for the triazole proton, a singlet (2H) at 7.24 ppm for NH_2, and a $-CH_2$ attached to the triazole ring at 5.61 ppm (2H) are seen. In the ^{13}C NMR, the peaks of carbonyl carbons are observed at about 190 and 163 ppm. The IR spectrum of the compound showed characteristic absorption bands at around 3266 cm^{-1} for NH_2, 3071 cm^{-1} for = C—H, and 1505 cm^{-1} for C═C. There are two peaks assigned to SO_2 as symmetric and asymmetric stretching. The peaks of asymmetric and symmetric stretch are appeared around 1350 and 1160 cm^{-1}, respectively. All spectra support the structure of the synthesized compounds.

2.2. Biological evaluation

2.2.1. Carbonic anhydrase inhibitory effect of the target compounds

The target 1,2,3-triazole benzenesulfonamide substituted 1,3-

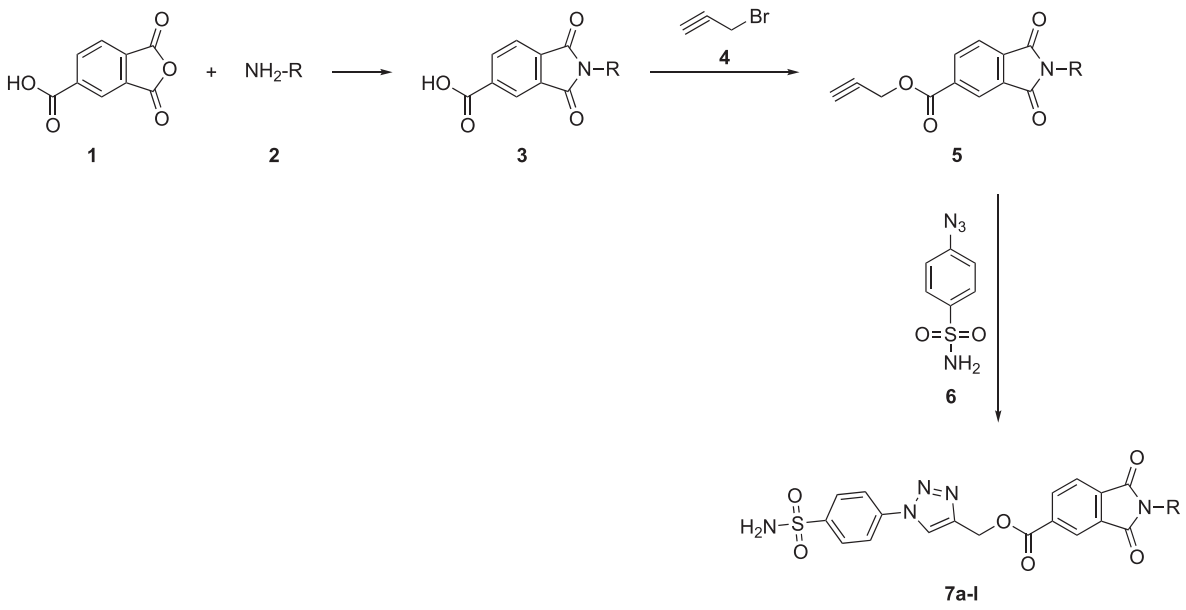

Compound ID	R	Compound ID	R	Compound ID	R
7a	Ph	**7e**	3-FPh	**7i**	Piperonyl
7b	2-ClPh	**7f**	2-IPh	**7j**	Octyl
7c	4-ClPh	**7g**	4-CNPh	**7k**	Hexyl
7d	2,6-diMePh	**7h**	Naphtyl	**7l**	Butyl

Scheme 2. Synthetic pathway of target 1,2,3-triazole based benzenesulfonamides **7a-l**.

dioxoisoindolin-5-carboxylate derivatives (**7a-l**) were tested as inhibitors of the five physiologically and pharmacologically relevant *h*CAs, the cytosolic *h*CA I and II, as well as the transmembrane isoforms *h*CA IV, IX, and XII, by an esterase assay. Acetazolamide (AAZ, PubChem CID: 1986) was included in the experiments as a standard inhibitor, as it is a clinically used drug despite lacking selectivity toward a particular *h*CA isoform. Enzyme inhibition constants (K_I) and their coefficient of determination (R^2) are reported in Table 1.

The off-target cytosolic isoform *h*CA I was potently inhibited by 1,2,3-triazole linked benzenesulfonamides **7a-l** with K_Is in the low

Table 1
Inhibition data of human CA isoforms *h*CA I, II, IV, IX, and XII with novel synthesized 1,2,3-triazole based benzenesulfonamides **7a-l** and the reference inhibitor acetazolamide, a clinically used drug.

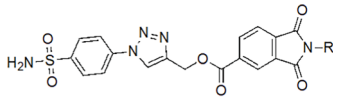

7a-l

Compounds		*h*CA I		*h*CA II		*h*CA IV		*h*CA IX		*h*CA XII	
ID	**R**	K_I[a] (nM)	R^2	K_I[a] (nM)	R^2	K_I[a] (nM)	R^2	K_I[a] (nM)	R^2	K_I[a] (nM)	R^2
7a	Ph	38.22 ± 7.27	0.9425	50.13 ± 6.29	0.9815	43.11 ± 5.79	0.9754	18.29 ± 3.60	0.9473	24.24 ± 3.19	0.9749
7b	2-ClPh	38.41 ± 7.54	0.9466	37.75 ± 7.32	0.9448	36.13 ± 3.59	0.9855	18.60 ± 2.96	0.9620	14.05 ± 2.13	0.9701
7c	4-ClPh	48.97 ± 6.39	0.9793	75.94 ± 12.00	0.9729	29.94 ± 5.14	0.9520	48.91 ± 8.48	0.9649	33.89 ± 4.45	0.9774
7d	2,6-diMePh	20.92 ± 2.60	0.9770	50.60 ± 10.83	0.9359	32.50 ± 3.23	0.9855	24.46 ± 4.19	0.9559	15.10 ± 2.14	0.9683
7e	3-FPh	48.12 ± 8.68	0.9564	9.72 ± 1.91	0.9516	18.28 ± 1.86	0.9839	22.85 ± 3.30	0.9692	19.72 ± 2.46	0.9799
7f	2-IPh	105.00 ± 10.63	0.9495	23.37 ± 3.38	0.9715	26.16 ± 2.74	0.9840	35.28 ± 5.43	0.9643	54.32 ± 3.40	0.9892
7 g	4-CNPh	25.17 ± 2.80	0.9821	16.87 ± 2.42	0.9713	34.96 ± 3.99	0.9805	28.56 ± 5.85	0.9364	14.39 ± 2.26	0.9637
7 h	Naphtyl	32.11 ± 4.36	0.9771	30.79 ± 5.65	0.9618	13.11 ± 1.48	0.9817	25.31 ± 4.42	0.9575	9.22 ± 1.40	0.9683
7i	Piperonyl	27.25 ± 4.41	0.9621	38.25 ± 5.57	0.9722	64.57 ± 10.74	0.9662	23.90 ± 3.02	0.9774	27.55 ± 3.34	0.9783
7j	Octyl	42.78 ± 7.58	0.9519	67.27 ± 13.16	0.9643	42.77 ± 6.26	0.9665	50.04 ± 5.81	0.9800	26.16 ± 3.73	0.9708
7 k	Hexyl	37.81 ± 7.40	0.9446	32.84 ± 4.96	0.9658	66.76 ± 13.87	0.9444	75.22 ± 15.26	0.9433	44.15 ± 6.12	0.9708
7 l	Butyl	34.99 ± 4.01	0.9805	35.79 ± 5.29	0.9733	25.08 ± 3.60	0.9703	35.01 ± 4.87	0.9725	33.46 ± 6.88	0.9344
AAZ[b]	–	451.80 ± 59.13	0.9398	327.30 ± 32.75	0.9712	354.90 ± 68.62	0.9267	437.20 ± 53.93	0.9420	338.90 ± 33.41	0.9688

[a] The test results were expressed as means of triplicate assays ± SEM.
[b] Acetazolamide.

nanomolar range of 20.92–105.00 nM, indicating that all synthesized compounds (**7a-l**) are higher selective and more potent inhibitors than reference drug AAZ (K_I of 451.80 nM). The most active derivatives in this series enclose 2,6-dimethylphenyl **7d**, 4-cyanophenyl **7g**, and piperonyl **7i** groups, which have K_Is of 20.92, 25.17, and 27.25 nM, respectively. Compounds having 3-fluorophenyl **7e** and 4-chlorophenyl **7c** groups exhibited K_Is of 48.12 and 48.97 nM, respectively, whilst the weakest inhibitor in this group, **7f**, which has a K_I of 105 nM, incorporates the 2-iodophenyl group.

Exploring the inhibitory effect of herein reported 1,2,3-triazolyl-1,3-dioxoisoindoline benzenesulfonamides (**7a-l**), all analogues showed potent inhibitory action towards the physiologically dominant off-target *h*CA II isoform with K_Is ranging from 9.72 to 75.94 nM, which is even better than the standard drug AAZ (K_I of 327.30 nM). In particular, 3-fluorophenyl analogue **7e** exhibited the best *h*CA II inhibitory effect with single-digit nanomolar activity (K_I of 9,72 nM). Also, analogues **7g** and **7f** had the potently *h*CA II inhibitory effect with two-digit nanomolar activities (K_Is of 16.87 and 23.37 nM, respectively), whereas **7c**, **7j**, and **7d** exerted the least activity with K_Is of 50.60, 67.27, and 75,94 nM, respectively.

The transmembrane isoform *h*CA IV was strongly inhibited by all 1,2,3-triazole based benzenesulfonamide derivatives **7a-l**, with K_I ranging between 13.11 nM and 66.76 mM, which is even better than the reference drug AAZ (K_I of 354.90 nM). Two derivatives **7h** and **7e** were found to be the most potent inhibitors among the synthesized compounds, with K_I constants less than 20 nM; namely, these analogues containing 2-naphthalene and 3-fluorophenyl moieties, respectively, were determined to be effective inhibitors of *h*CA IV. Also, piperonyl **7i** and 2-hexyl **7k** analogues were the weakest inhibitors of *h*CA IV, with K_Is of 64.57 and 66.76 nM, respectively, in this series.

All the synthesized 1,2,3-triazolyl-1,3-dioxoisoindoline benzenesulfonamide analogues **7a-l** strongly inhibited the transmembrane tumor-associated target isoform *h*CA IX, with two-digit K_Is of 18.29–75.22 nM. The 2-phenyl **7a**, 2-chlorophenyl **7b**, and 3-fluorophenyl **7e** analogues showed a robust inhibitory effect with K_Is of 18,29, 18,60, and 22,85 nM, respectively, compared to standard drug AAZ (K_I of 437.20 nM). Also, 2-iodophenyl **7f** (K_I of 35.28 nM) displayed an equipotent activity relative to the 2-butyl **7l** analogue (K_I of 35.01 nM). The 4-chlorophenyl **7c**, 2-octyl **7j**, and 2-hexyl **7k** analogues (K_Is of 48.91, 50.04, and 75.22 nM) recorded the least inhibiting activity in the group.

The target compounds, 1,2,3-triazole linked benzenesulfonamide compounds **7a-l**, strongly inhibited the transmembrane tumor-associated another target isoform *h*CA XII, with single/two-digit K_I ranging from 9.22 to 54.32 nM compared to the reference drug AAZ (K_I of 338.90 nM). Five analogues, 2-naphthalene **7h**, 2-chlorophenyl **7b**, 4-cyanophenyl **7g**, 2,6-dimethylphenyl **7d**, and 3-fluorophenyl **7e** exhibited potent inhibition of *h*CA XII with K_I constants less than 20 nM, whereas 2-iodophenyl **7f** analogue was the weakest inhibitor (K_I of 54.32 nM).

2.2.2. Sars parameters of the target compounds

The following structure–activity relationships (SARs) were acquired from the results presented in Tables 1 and 2.

Regarding SAR, derivatives **7d** and **7e**, having a 2,6-dimethylphenyl and 3-fluorophenyl moiety and have K_Is of 20.92 nM (*h*CA I) and 9.72 nM (*h*CA II), were found to be 1.83 and 5.15 times more effective than its unsubstituted phenyl analogue **7a** respectively, which has K_Is of 38.22 nM (*h*CA I) and 50.13 nM (*h*CA II). Substituting phenyl ring with halogens such as 2-chloride **7b** with K_I of 38.41 nM, 4-chloride **7c** with K_I of 48.97 nM, 3-fluoride **7e** with K_I of 48.12 nM, and 2-iodide **7f** with K_I of 105.00 nM resulted in lower activity against *h*CA I. Also, the reduction of the K_I constants was observed when the linear alkyl chains were elongated as in 2-butyl **7l**, 2-hexyl **7k**, and 2-octyl **7j** analogues (K_I values of 34.99, 37.81, and 42.78 nM, respectively). When compared to unsubstituted phenyl analogue **7a**, 4-cyano bearing phenyl compound **7g** (K_Is of 25.17 and 16.87 nM, respectively) increased activity towards *h*CAI and *h*CA II than halogen bearing phenyl analogues **7b**, **7c**, **7e**, and **7f**.

Table 2
Selectivity indexes for the inhibition of transmembrane human CA isoforms *h*CA IV, IX, and XII over *h*CA I and II for targeted 1,2,3-triazole based benzenesulfonamides **7a-l**.

Compounds ID	Selectivity index[a]					
	I/IV	II/IV	I/IX	II/IX	I/XII	II/XII
7a	0.89	1.16	2.09	2.74	1.58	2.07
7b	1.06	1.04	2.07	2.03	2.73	2.69
7c	1.64	2.54	1.00	1.55	1.44	2.24
7d	0.64	1.56	0.86	2.07	1.39	3.35
7e	2.63	0.53	2.11	0.43	2.44	0.49
7f	4.01	0.89	2.98	0.66	1.93	0.43
7 g	0.72	0.48	0.88	0.59	1.75	1.17
7 h	2.45	2.35	1.27	1.22	3.48	3.34
7i	0.42	0.59	1.14	1.60	0.99	1.39
7j	1.00	1.57	0.85	1.34	1.64	2.57
7 k	0.57	0.49	0.50	0.44	0.86	0.74
7 l	1.40	1.43	1.00	1.02	1.05	1.07

[a] Selectivity index (S_I) of inhibitors for transmembrane *h*CA IV, IX, and XII over off-targets isoforms, *h*CA I and II, calculated as the ratio of K_I off-target *h*CA/K_I target *h*CA. A potent, selective inhibitor is characterized by a high-value ratio.

Replacing the phenyl ring (**7a**, K_I of 43.11 nM) with a non-fused heterocycle raised the inhibitory effect against the transmembrane isoform *h*CA IV by 3.29 times, as seen in the naphthalene analogue **7h** (K_I of 13.11 nM). Also, the introduction of electron-withdrawing (2-chloro **7b**, 4-chloro **7c**, 3-fluoro **7e**, 2-iodide **7f**, and 4-cyano **7g** analogues) or -donating (2,6-dimethyl **7d**) groups increased inhibitory action against *h*CA IV, and these analogues exhibited low nanomolar range K_Is, in the range of 18.28–36.13 nM.

The presence of both the electron-withdrawing groups (2-chloro **7b**, 4-chloro **7c**, 3-fluoro **7e**, 2-iodide **7f,** and 4-cyano **7g** analogues) or the bulky electron-donating 2,6-dimethylphenyl group (**7d**) resulted in a decrease of affinity against the tumor-associated isoform *h*CA IX when compared to the unsubstituted phenyl (**7a**, K_I of 43.11 nM). Also, replacing the phenyl ring **7a** with heterocycles such as naphthalene **7h** (K_I of 25.31 nM) and piperonyl **7i** (K_I of 23.90 nM) significantly decreased the inhibitory effect against *h*CA IX. Furthermore, having or elongation of the linear alkyl chains in 2-butyl **7l**, 2-octyl **7j**, and 2-hexyl **7k** analogues led to decreased inhibitory effect (K_Is of 35.01, 50.04, and 75.22 nM, respectively) towards *h*CA IX isoform.

As previously discussed for *h*CA IV, this series also did not show a notably different kinetic profile for the *h*CA XII isoform, and the profile was almost similar. Replacing the phenyl ring (**7a**, K_I of 24.24 nM) with a non-fused heterocycle raised the inhibitory effect towards the tumor-associated isoform *h*CA XII by 2.62 times, as in the naphthalene analogue **7h** (K_I of 9.22 nM). Also, the presence of either electron-donating groups such as methyl (**7d**, K_I of 15.10 nM) or electron-withdrawing groups such as 2-chloro (**7b**, K_I of 14.05 nM), 3-fluoro (**7e**, K_I of 19.72 nM), and 4-cyano (**7g**, K_I of 14.39 nM) at the *ortho*, *meta*, or *para*-position of the phenyl ring increased the inhibitory effect against *h*CA XII (**7c** and **7f** were an exception). Further elongation of **7a** by alkyl chains (as in compounds **7j**, **7l**, and **7k**) or replacing the phenyl with piperonyl group (as in compound **7i**, K_I of 27.55 nM) resulted in a lower *h*CA XII inhibition with K_I of 26.16, 33.46, and 44.15 nM, respectively.

2.2.3. Selectivity parameters of the target compounds

Given that their primary sequences are similar to more than 30 % of one another, the *h*CAs are highly closely related. Due to the fact that the majority of the sequence identity corresponds to residues found in the *h*CAs active site, this similarity makes it challenging to design *h*CAIs that are isoform-selective.[42] Synthesized 1,2,3-triazole benzenesulfonamide substituted 1,3-dioxoisoindolin-5-carboxylates (**7a-l**) developed notable selectivity against the transmembrane target isoforms (*h*CA IV, IX, and

XII) over the off-target isoforms (*h*CA I and II). The selectivity index (S_I) was computed by the ratio between the K_I for *h*CA I and II relative to *h*CA IV, IX, and XII and were used to indicate enzyme selectivity, as observed in Table 2.

Regarding selectivity towards *h*CA IX over the off-target isoform *h*CA I, the determined S_I I/IX for 1,2,3-triazole linked benzenesulfonamides **7a-l** were ranged from 2.98 to 0.50. Six analogues displayed S_I (2.98–1.14) higher than the standard drug AAZ value (S_I of 1.03). Analogue **7f** with a 2-iodophenyl showed selectivity towards *h*CA IX, S_I of 2.98 (2.89-times that of AAZ). The presence of a small strong electron-withdrawing group, 3-fluoro substituent, in **7e** reflected negatively on selectivity with a lower S_I of 2.11. More extensive electron-withdrawing groups, such as 2-chloride **7b** and 4-chloride **7c** analogues, decreased mainly the selectivity with listed lower S_I values of 2.07 and 1.00, respectively. The presence of electron-donating groups like the 2,6-dimethyl in **7d** lowered markedly the selectivity, S_I of 0.86. The presence of the cyano group on **7 g** much reduced the selectivity (S_I of 0.88) relative to the non-substituted **7a** (S_I of 2.09). Replacement of the phenyl group with a more lipophilic great naphthyl or piperonyl group in **7h** and **7i** decreased the selectivity (S_I values of 1.27 and 1.14, respectively). Furthermore, having or elongating the linear alkyl chains as in the analogues **7l**, **7k**, and **7j** led to reduced selectivity (S_I values of 1.00, 0.85, and 0.50, respectively) over standard drug AAZ.

Concerning selectivity towards *h*CA XII over the off-target isoform *h*CA I, the calculated S_I I/XII for 1,2,3-triazole linked benzenesulfonamide analogues **7a-l** ranged from 3.48 to 0.86. Nine analogues displayed S_I (3.48–1.39) higher than the standard drug AAZ (S_I of 1.33). Analogue **7a** with a phenyl group displayed a high selectivity towards *h*CA IX, S_I of 1.58 (1.19-times that of AAZ). Strong electron-withdrawing in the *ortho*- or *meta*-position halogens, chloride **7b**, fluoride **7e**, and iodide **7f** raised selectivity with S_I of 2.73, 2.44, and 1.93, respectively. The cyano substituent in **7g** slightly raised the selectivity (S_I of 1.75). Replacement of the phenyl group with a more lipophilic great naphthyl group in **7h** enhanced the selectivity, recording the best S_I of 3.48.

Target 1,2,3-triazole linked benzenesulfonamides **7a-l** exhibited selectivity towards *h*CA IX over the off-target isoform *h*CA II, with S_I II/IX from 2.74 to 0.43 relative to reference drug AAZ, S_I of 0.75. Analogue **7a** with a phenyl group showed the highest selectivity towards *h*CA IX, S_I of 2.74 (3.65-times that of AAZ). Chemical modifications to the structure of analogue **7a** resulted in decreasing selectivity. The substituent of a 2,6-dimethyl group in **7d** to the phenyl group (S_I of 2.07) reduced selectivity. The remaining six analogues showed lower selectivity with S_I values between 2.03 and 1.02.

In relation to selectivity towards *h*CA XII over the off-target isoform *h*CA II, nine analogues exhibited higher selectivity with S_I II/XII from 3.35 to 1.07 compared to reference drug AAZ, S_I of 0.97. The presence of electron-donating groups like the 2,6-dimethyl in **7d** showed the highest selectivity towards *h*CA XII with S_I value of 3.35 (3.45-times that of AAZ). Replacement of the phenyl group (**7a**) with a more lipophilic great naphthyl group in **7h** and linear octyl chain in **7j** raised the selectivity (S_I of 3.34 and 2.57, respectively). Chemical modifications on the structure of compound **7a** resulted in differing selectivity. The 2-chlorophenyl **7b** (S_I of 2.69) and 4-chlorophenyl **7c** (S_I of 2.24) showed a high selectivity whilst the 4-cyanophenyl **7g** (S_I of 1.17), 3-fluorophenyl **7e** (S_I of 0.49), and 2-iodophenyl **7f** (S_I of 0.43) reported the low selectivity. The remaining three analogues showed variable selectivity ranging from, a high S_I of 1.39 for the piperonyl analogue **7i** to a poor S_I of 0.74 recorded for **7k** bearing the hexyl chain.

In conclusion, the above findings conclude that the selectivity profile of *h*CAs was powerfully touched, and highly selective drug candidates were developed. 2-Iodophenyl (**7f**), and 2-naphthyl (**7h**) analogues (over off-target *h*CA I) and phenyl (**7a**) and 2,6-dimethylphenyl (**7d**) analogues (over off-target *h*CA II) exhibited the best selectivity for tumor isoforms *h*CA IX and XII, respectively. The most potent analogues **7a** (K_I of 18.29 nM for *h*CA IX) and **7h** (K_I of 9.22 nM for *h*CA XII) exhibited a good selectivity profile, S_I values of 2.09, and 2.74 (*h*CA IX over off-target *h*CAs I and II, respectively) and 3.48, and 3.34 (*h*CA XII over off-target *h*CAs I and II, respectively). Also, incorporating the lipophilic great naphthyl tail in the target 1,2,3-triazole benzenesulfonamide substituted 1,3-dioxoisoindolin-5-carboxylate analogues improved both the *h*CA inhibitory effect and selectivity activity against the transmembrane tumor-associated target isoform *h*CA XII.

Numerous 1,2,3-triazole-containing sulfonamides have been the subject of much research to find potent and selective inhibitors. In order to identify innovative and selective target-oriented anticancer drug candidates, many 1,2,3-triazole compounds were synthesized by several research groups and evaluated as antitumor agents through their *h*CAs inhibition profile. According to Pala, *et al.*,[43] a series containing substituted triazolylbenzenesulfonamides were synthesized utilizing a click-tailing strategy. The cytosolic isoforms *h*CA I and II were poor inhibitors of all novel compounds endowed with various tail groups. Low nanomolar inhibitors of *h*CA IX and XII demonstrated remarkable selectivity over *h*CA I and II. When 4-[4-(4-pentylphenyl)-1*H*-1,2,3-triazol-1-yl]benzenesulfonamide (**4d**) and 4-[4-(2-bromoethyl)-1*H*-1,2,3-triazol-1-yl]benzenesulfonamide (**4e**) with a substituted triazolyl tail group were combined, they inhibited *h*CA IX more selectively than *h*CA I and II by 640, 151, and 181.2, respectively. Furthermore, these compounds also selectively inhibited *h*CA XII with the selectivity of 258.1-, 60.9-fold, and 500-, 56.8-fold over *h*CA I and II, respectively. However, compound **54** had the most inhibition across the series. Moreover, Sharma, *et al.*[44] designed and synthesized various unique hydroxy-trifluoromethylpyrazoline-carbonyl-1,2,3-triazoles (**9**–**12**) and trifluoromethylhydrazone-carbonyl-1,2,3-triazoles (**13**) bearing benzenesulfonamide, which were tested for their *h*CAs inhibition profiles. Many demonstrated potent suppression of the *h*CA IX and XII isoforms, and some displayed selectivity for these tumor-associated isoforms over the prevalent major off-target isoforms, *h*CA I and II, to significant degrees. Salmon, *et al.*[45] reported that the tail approach was used to create several metallocene-based *h*CAIs that used triazole moiety as a linker. Even though several of the derivatives had vigorous anti-*h*CA IX/XII activity, they lacked the selectiveness for these isoforms over *h*CA I and II. 3-(4-Ferrocenyl-1*H*-1,2,3-triazol-1-yl)benzenesulfonamide (**5**), which contains a triazole-ferrocene tail, was the only one in the series to effectively inhibit both *h*CA IX and XII (K_Is of 33.1 nM and 18.8 nM, respectively), as well as to show a respectable selectivity ratio of 54.1 and 95.2 for *h*CA IX and XII over *h*CA I and of 125.8 and 221.5 for *h*CA IX and XII.

2.2.4. Antiproliferative activity of the target compounds

The diagnosis and therapy of tumors have attracted the most interest among the possible clinical uses of *h*CAIs over the past ten years.[46] Overexpression of the *h*CA IX and XII isoforms is a potent marker of malignant tissues in multiple investigations.[47–48] As a result, various tumor-visualization agents have been created, based either on biomolecules that target *h*CA IX and XII isoforms or on small compounds that include sulfonamide.[49] Additionally, their catalytic activity significantly assures that tumor cells can adapt to unfavorable growth conditions, including hypoxia and food deprivation.[50] In particular, the extracellular domain of these isoenzymes has a catalytic activity that is crucial for the operation of several transport proteins and prevents intracellular acidosis.[51–52].

To this end, because of their favorable selectivity profile towards *h*CA IX and XII isoforms, the antiproliferative activity of a series of 1,2,3-triazole benzenesulfonamide substituted 1,3-dioxoisoindolin-5-carboxylate was studied on a panel of human lung (A549) adenocarcinoma cell line used the protocol of the MTT assay. Doxorubicin (DOX, PubChem CID: 31703) was utilized as a reference cytotoxic drug, and IC_{50} values of the agents' anti-cancer activity are listed in Table 3. Investigating the MTT assay results highlighted that the tested analogues (**7a-l**) exhibited moderate growth inhibitory effect against the A549 cell line with IC_{50} ranging from 129.71 to 352.26 μM. Interestingly, the most active analogue in this series was **7i** containing 2-piperidine, which has

Table 3
IC_{50} values of the novel synthesized 1,2,3-triazole based benzenesulfonamides **7a-l** and the reference inhibitor doxorubicin, a clinically used anticancer drug toward human lung (A549) adenocarcinoma cell line.

Compounds ID	IC_{50}[a] (μM)
7a	299.60 ± 11.64
7b	289.67 ± 11.01
7c	352.26 ± 8.88
7d	253.39 ± 18.96
7e	230.51 ± 12.13
7f	257.62 ± 2.98
7 g	266,30 ± 6.62
7 h	278,41 ± 8.00
7i	129,71 ± 3.15
7j	234,90 ± 5.69
7 k	160,66 ± 3.03
7 l	198,51 ± 7.79
DOX[b]	10.83 ± 0.40

[a] The test results were expressed as means of triplicate assays ± SD.
[b] Doxorubicin.

an IC_{50} value of 129.71 μM compared to reference drug DOX (IC_{50} of 10.83 μM). Also, analogues **7k** and **7l** inhibited the growth of A549 with IC_{50}s of 160.66 and 198.51 μM, respectively, whereas **7b**, **7a**, and **7c** had the lowest activity with three-digit micromolar activities (IC_{50}s of 289.67, 299.60, and 352.26 μM, respectively).

2.3. In silico study

With the use of the X-ray crystallographic structures of the *h*CA I (PDB ID 1AZM), *h*CA II (PDB ID 3HS4), *h*CA IV (PDB ID 5JN8), *h*CA IX (PDB ID 3IAI), and *h*CA XII (PDB ID 1JD0) isoforms, the newly synthesized compounds', 1,2,3-triazole benzenesulfonamide substituted 1,3-dioxoisoindolin-5-carboxylate analogues binding patterns were examined. The co-crystallized native ligand AZM (5-acetamido-1,3,4-thiadiazole-2-sulfonamide, AAZ) was re-docked in the center of the enzyme binding sites to confirm the validity of the docking setup. The minimal RMSD values (0.21, 1.02, 1.37, 1.29, and 1.33, respectively) and the ability of the docking poses of the co-crystalized ligands to reproduce all of the essential interactions demonstrated the viability of the used docking methodology for the intended docking study during the re-docking validation process. The binding mechanisms of the newly developed analogues in these *hCA*s' active sites were subsequently examined using the validated setup. The most potent inhibitors, **7d** (for *h*CA I), **7e** (for *h*CA II), **7h** (for *h*CA IV and XII), and **7a** (for *h*CA IX), showed potent binding affinity to the *h*CA isoforms with predicted docking scores in *h*CA I (Xp GScore of –7.28 kcal/mol and MM-GBSA value of –32.77 kcal/mol), *h*CA II (Xp GScore of –8.51 kcal/mol and MM-GBSA value of –38.10 kcal/mol), *h*CA IV (Xp GScore of –5.28 kcal/mol and MM-GBSA value of –16.63 kcal/mol), *h*CA IX (Xp GScore of –2.76 kcal/mol and MM-GBSA value of 0.24 kcal/mol), and *h*CA XII (Xp GScore of –6.83 kcal/mol and MM-GBSA value of –17.45 kcal/mol). The novel synthesized analogues demonstrated comparable binding patterns in *h*CA isoforms, which include the accommodation of the sulfonamide moiety deeply in the active site interacting with the active site Zn^{2+} ion and by hydrogen bonding with the gatekeeper residues Thr199 (distances of 1.75 Å for *h*CA I, 1.95 Å for *h*CA II, 1.99 Å for *h*CA IV and *h*CA IX, and 2.59 Å for *h*CA XII) and Thr200 (distance of 2.52 Å for *h*CA II).

In *h*CA II, 1,3-dioxoisoindoline moiety makes a hydrogen bond with Phe131 in the center of the active site, while two water molecules interact through hydrogen bonding at distances of 2.15 and 2.18 Å by an oxygen atom and carbonyl group. 1,2,3-Triazole moiety is involved in a hydrophobic interaction with the hydrophobic side chains of residues Phe91 in *h*CA I, Phe131 in *h*CA II, and Trp5 in *h*CA IX. In *h*CA IV and *h*CA XII, the benzene ring of hydrophobic tail 1,3-dioxoisoindoline-5-carboxylate and residues His64 and Trp5, respectively, form a pi-pi stacking interaction. On the other side, a benzenesulfonamide phenyl ring with polar residue His94 interacts through pi-pi stacking in *h*CA XII (Figures 1-5). The novel developed 1,2,3-triazole benzenesulfonamide substituted 1,3-dioxoisoindolin-5-carboxylate analogues demonstrated different affinity and selectivity patterns in each *h*CA, as indicated by the docking scores for the investigated *h*CAs. This was due to their various structural variations, which give them a variety of steric and electronic properties.

Moreover, the chemical drug-likeness of targeted 1,2,3-triazole based benzenesulfonamides **7a-l** was assessed using the QikProp module[53] of the Schrödinger Suite 2022-3 for Mac, wherein the selected ADME/T (absorption, distribution, metabolism, elimination, and toxicity) parameters were computed and listed in Table 4. It is evident that the analogues **7a-l** under investigation displayed drug-like traits based on physicochemical properties, and all the compounds (**7a-l**) comply with Lipinski's five[54] and Jorgensen's three[55] rules.

3. Conclusion

A newly series of 1,2,3-triazole benzenesulfonamide substituted 1,3-dioxoisoindolin-5-carboxylate (**7a-l**) was designed in the current study using the tail method. This was accomplished through the molecular hybridization of the zinc-binding 4-benzenesulfonamide moiety with the 1,2,3-triazole scaffold. However, the 1,3-dioxoisoindoline-5-carboxylate was used to build the hydrophobic tail. The inhibitory action of the designed and synthesized analogues was tested against five different *h*CA isoforms, including *h*CA I, II, IV, IX, and XII. The most potent of the developed substances against *h*CA II was 3-fluorophenyl analogue **7e** (K_I of 9.72 nM). Compared to AAZ (K_I of 437.20 nM), compound **7a** (K_I of 18.29 nM) had significantly more potent inhibitory action against tumor-associated isoform *h*CA IX. Another tumor-associated isoform *h*CA XII was more effectively inhibited by compound **7h** (K_I of 9.22 nM) than by AAZ (K_I of 338.90 nM). 2-Iodophenyl (**7f**, S_I of 2.98), and 2-naphthyl (**7h**, S_I of 3.48) analogues (over off-target *h*CA I) and phenyl (**7a**, S_I of 2.74) and 2,6-dimethylphenyl (**7d**, S_I of 3.35) analogues (over off-target *h*CA II) exhibited a remarkable selectivity for tumor isoforms *h*CA IX and XII, respectively. Nevertheless, adding the lipophilic large naphthyl tail to the 1,3-dioxoisoindolin-5-carboxylate analogues of the target 1,2,3-triazole benzenesulfonamide increased both the *h*CA inhibitory effect and selective activities against the target isoform, *h*CA XII. Moreover, findings from the MTT experiment showed that the analogus (**7a-l**) had considerable growth inhibitory action against the human lung (A549) adenocarcinoma cell line, with concentrations ranging from 129.71 to 352.26 μM. Molecular docking of these 1,2,3-triazole based benzenesulfonamide analogues in the *h*CAs active sites evidences the accommodation of the sulfonamide moiety deeply in the active site interacting with the active site Zn^{2+} ion and by hydrogen bonding with the key residue Thr199.

4. Materials and methods

4.1. General procedure for the preparation of the target compounds

All the chemicals and solvents used during the study were purchased from Sigma-Aldrich and used without further purification. Melting points were determined by Yanagimoto micro-melting point apparatus and uncorrected. The mass analysis was carried out with a LC-MS QTOF-9030 spectroscopy. Infrared spectra were measured on a Shimadzu Prestige-21 (200 VCE) spectrometer. ^{1}H, and ^{13}C NMR spectra were obtained using VARIAN Infinity Plus at 300 and 75 Hz, respectively. All analogues (**7a-l**) are greater than 95 % pure according to LC-MS analysis, and their traces are provided in the Supporting Information.

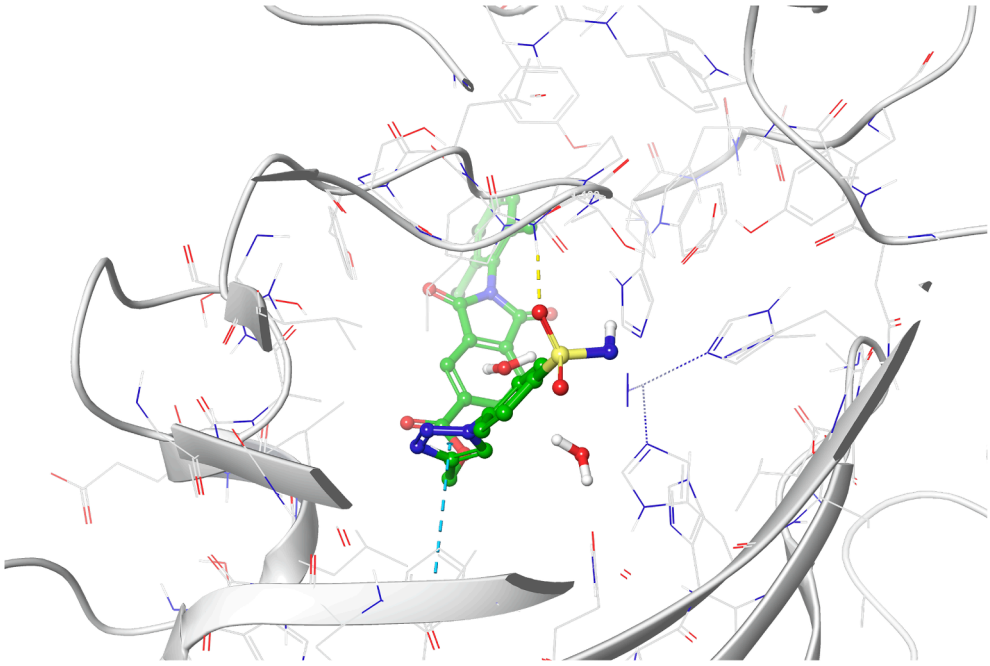

A

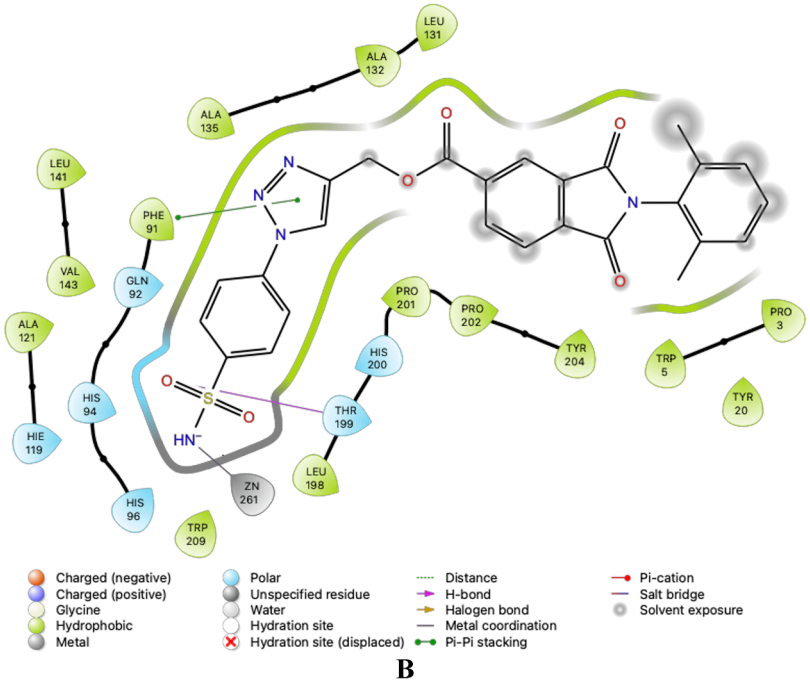

B

Figure 1. Molecular docking of *h*CA I isoform (PDB ID 1AZM) with [1-(4-sulfamoylphenyl)-1*H*-1,2,3-triazol-4-yl]methyl 2-(2,6-dimethylphenyl)-1,3-dioxoisoindoline-5-carboxylate (**7d**). **(A)** 3D docking pose of analogue **7d** within the binding pocket of 1AZM. In the 3D panel, hydrogen bonds and pi-pi stacking interactions are shown in yellow and blue dashed lines, respectively. Only the interacting amino acids are demonstrated for the sake of clarity. **(B)** 2D interaction diagram of 1AZM with analogue **7d**. (For interpretation of the references to colour in this figure legend, the reader is referred to the web version of this article.)

4.1.1. General procedure for preparation of compounds 3a-l

A mixture of (1,3-dioxo-1,3-dihydrobenzofuran-5-carboxylic acid) compound **1** (2 mmol) and compound **2** (2 mmol) in acetic acid (10 ml) was reflux at 100 °C for 6 h. After the reaction was completed, the reaction mixture was cooled to room temperature, and ice water was added to it with stirring for 30 min (if the reaction did not precipitate, K_2CO_3 solution was added slowly), and the separated solid was filtered and then dried.

4.1.2. General procedure for preparation of compounds 5a-l

Compound **3** (1 mmol) was dissolved in DMSO (5 ml) with the addition of K_2CO_3 (2 mmol), a catalytic amount of TBAB, and compound **4**, 1 mmol propargyl bromide at room temperature for 6 h. After the reaction was completed, ice water was added to it and stirred for 30 min. The separated solid was filtered, then dried.

4.1.3. Synthesis of 4-azidobenzenesulfonamide (6)

4-Aminobenzenesulfonamide (5 g) was dissolved in HCl (6.0 M) and stirred at 0 °C in an ice bath until complete solubility. Sodium nitrite (2.5 g) was dissolved in cold water and added to the reaction. After complete addition, it waited 1 h, and sodium azide (2.8 g) was added slowly to the reaction. The reaction was stirred at room temperature overnight. After the reaction, the separated solid was filtered and dried.

4.1.4. General procedure for preparation of targeted compounds 7a-l

Compound **5** (1 mmol) was dissolved in DMF (5 ml) with the

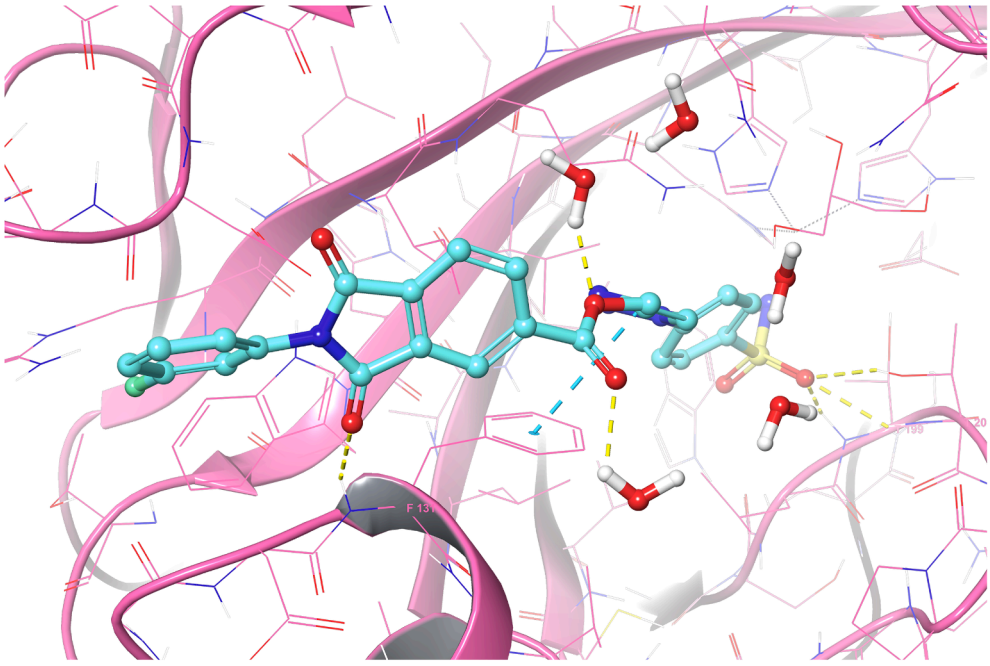

A

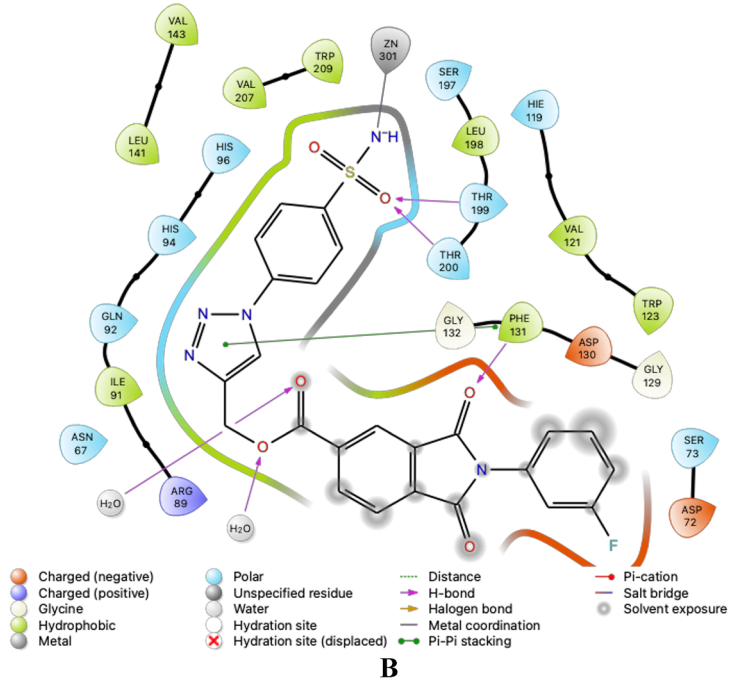

B

Figure 2. Molecular docking of *h*CA II isoform (PDB ID 3HS4) with analogue [1-(4-sulfamoylphenyl)-1*H*-1,2,3-triazol-4-yl] methyl 2-(3-fluorophenyl)-1,3-dioxoisoindoline-5-carboxylate (**7e**). **(A)** 3D docking pose of analogue **7e** within the binding pocket of 3HS4. In the 3D panel, hydrogen bonds and pi-pi stacking interactions are shown in yellow and blue dashed lines, respectively. Only the interacting amino acids are demonstrated for the sake of clarity. **(B)** 2D interaction diagram of 3HS4 with analogue **7e**. (For interpretation of the references to colour in this figure legend, the reader is referred to the web version of this article.)

addition of compound **6,** 1 mmol (4-azidobenzenesulfonamide) and (8 mmol $CuSO_4{\cdot}5H_2O$ with 1 mmol sodium ascorbate was reflux at 90 °C for 2 h. After completion, the reaction was cooled to room temperature, ice water was added to it, and the mixture was neutralized with concentrated HCl, which led to the precipitation of a solid with stirring for 30 min. The solid was filtered, washed with water, and then dried. The final targeted products were purified by crystallization from acetone-hexane. The prepared compounds shown in Scheme 2 were characterized by ^{1}H NMR, ^{13}C NMR, FT-IR, and mass spectrometry.

4.1.4.1. [1-(4-Sulfamoylphenyl)-1H-1,2,3-triazol-4-yl]methyl 1,3-dioxo-2-phenylisoindoline-5-carboxylate (7a). Pink solid, yield 91 %, m.p. 204 °C; ^{1}H NMR (300 MHz, DMSO-d_6) δ (ppm): 9.11 (s, 1H, H-Ar), 8.45 (d, 1H, H-Ar), 8.34 (d, 1H, H-Ar), 8.14 (s, 1H, H-triazole), 8.11 (d, 2H, H-Ar), 8.04 (d, 2H, H-Ar), 7.60–7.25 (m, 3H, H-Ar), 7.53 (s, 2H, –NH_2), 7.46 (d, 2H, H-Ar), 5.60 (s, 2H, –CH_2). ^{13}C NMR (75 MHz, DMSO-d_6) δ (ppm): 166.82, 164.75, 144.66, 143.72, 139.17, 136.31, 136.11, 135.50, 132.82, 132.35, 129.60, 128.98, 128.20, 127.99, 124.67, 124.24, 124.11, 121.19, 59.20. IR (ν, cm^{-1}): 3371 (NH_2), 3153 (=C—H), 1775 (C═O), 1098 (C—O), 1352 and 1161 (SO_2). QTOF LC-MS (m/zfound: (M−H): 502.0811; calculated [$C_{24}H_{21}N_5O_6S$]: 503.4907 [M]$^-$.

4.1.4.2. [1-(4-Sulfamoylphenyl)-1H-1,2,3-triazol-4-yl]methyl 2-(2-chlorophenyl)-1,3-dioxoisoindoline-5-carboxylate (7b). White solid, yield 49 %, m.p. 195 °C; ^{1}H NMR (300 MHz, DMSO-d_6) δ (ppm): 9.10 (s, 1H, H-Ar), 8.51 (d, 1H, H-Ar), 8.43 (d, 1H, H-Ar), 8.17 (s, 1H, H-triazole), 8.14

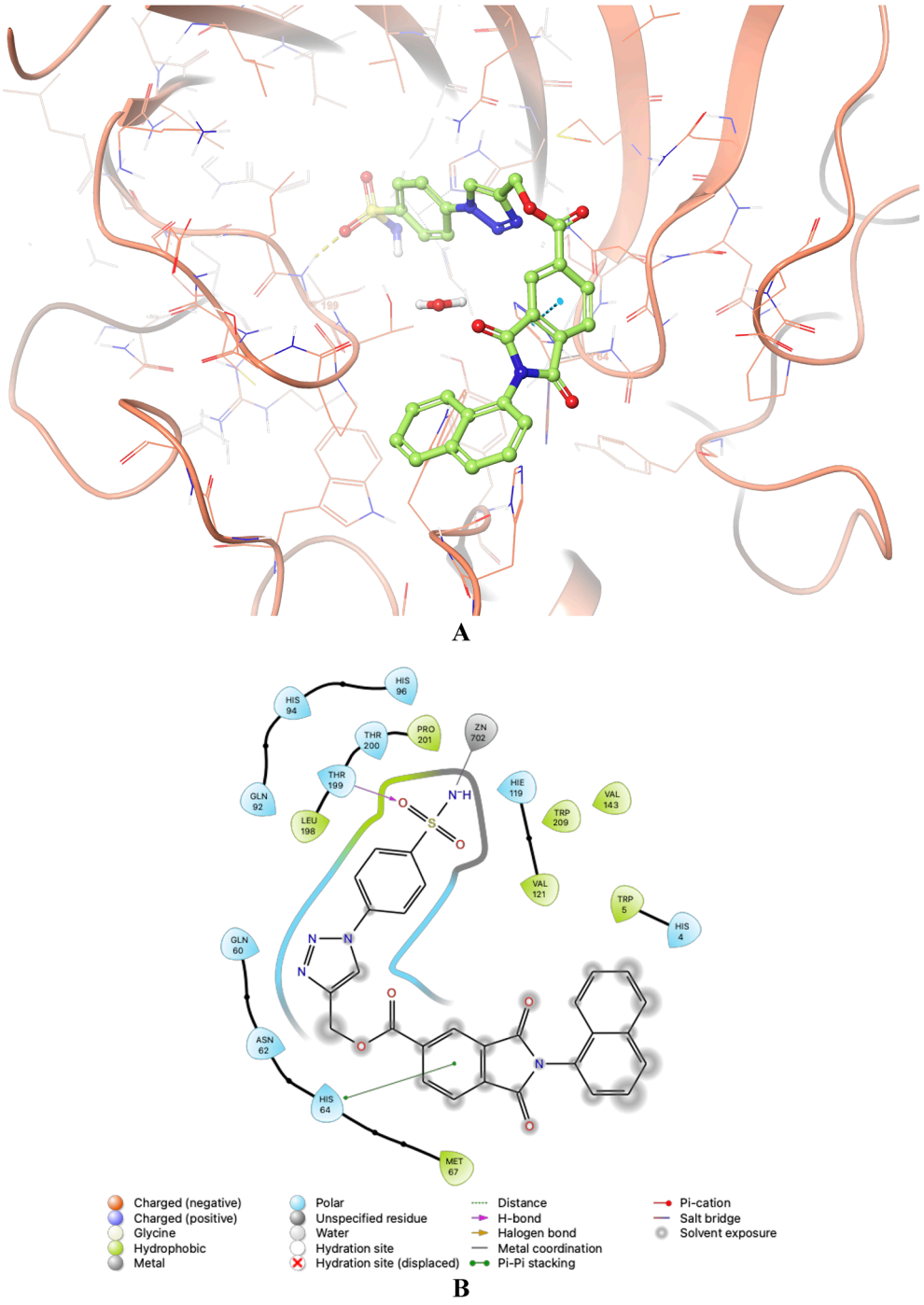

Figure 3. Molecular docking of *h*CA IV isoform (PDB ID 5JN8) with [1-(4-sulfamoylphenyl)-1*H*-1,2,3-triazol-4-yl]methyl 2-(naphthalen-1-yl)-1,3-dioxoisoindoline-5-carboxylate (**7h**). **(A)** 3D docking pose of analogue **7h** within the binding pocket of 5JN8. In the 3D panel, hydrogen bonds and pi-pi stacking interactions are shown in yellow and blue dashed lines, respectively. Only the interacting amino acids are demonstrated for the sake of clarity. **(B)** 2D interaction diagram of 5JN8 with analogue **7h**. (For interpretation of the references to colour in this figure legend, the reader is referred to the web version of this article.)

(d, 2H, H-Ar), 8.04 (d, 2H, H-Ar), 7.74 (t, 1H, H-Ar), 7.71 (t, 1H, H-Ar), 7.68 (d, 1H, H-Ar), 7.54 (d, 1H, H-Ar), 7.57 (s, 2H, –NH_2), 5.63 (s, 2H, –CH_2). ^{13}C NMR (75 MHz, DMSO-d_6) δ (ppm): 166.11, 164.63, 144.66, 143.74, 139.17, 136.71, 135.79, 132.77, 132.57, 132.06, 131.98, 130.65, 129.98, 128.96, 125.12, 124.55, 124.21, 121.19, 59.37. IR (ν, cm^{-1}: 3225 (NH_2), 3011 (=C—H), 1779 (C=O), 1095 (C—O), 1347 and 1163 (SO_2). QTOF LC-MS (m/zfound: (M−H): 536.0416; calculated [$C_{24}H_{16}ClN_5O_6S$]: 537.9354 [M]$^-$.

4.1.4.3. [1-(4-Sulfamoylphenyl)-1H-1,2,3-triazol-4-yl]methyl 2-(4-chlorophenyl)-1,3-dioxoisoindoline-5-carboxylate (7c). Brown solid, yield 28 %, m.p. 229 °C; ^{1}H NMR (300 MHz, DMSO-d_6) δ (ppm): 9.13 (s, 1H, H-Ar), 8.45 (d, 1H, H-Ar), 8.35 (d, 1H, H-Ar), 8.18 (s, 1H, H- triazole), 8.14 (d, 2H, H-Ar), 8.04 (d, 2H, H-Ar), 7.70–7.60 (m, 6H, H-Ar, –NH_2), 5.60 (s, 2H, –CH_2). ^{13}C NMR (75 MHz, DMSO-d_6) δ (ppm): 166.60, 164.72, 144.63, 143.70, 136.38, 136.08, 135.39, 133.43, 131.24, 129.68, 128.20, 124.75, 124.25, 12.14, 121.18, 59.30. IR (ν, cm^{-1}: 3071 (=C—H), 3261 (NH_2), 1785 (C=O), 1092 (C—O), 1348 and 1152 (SO_2). QTOF LC-MS (m/zfound: (M−H): 536.0417; calculated [$C_{24}H_{16}ClN_5O_6$]: 537.9354 [M]$^-$.

4.1.4.4. [1-(4-Sulfamoylphenyl)-1H-1,2,3-triazol-4-yl]methyl 2-(2,6-dimethylphenyl)-1,3-dioxoisoindoline-5-carboxylate (7d). Pink solid, yield 50 %, m.p. 173 °C; ^{1}H NMR (300 MHz, DMSO-d_6) δ (ppm): 9.12 (s, 1H, H-Ar), 8.51 (d, 1H, H-Ar), 8.40 (d, 1H, H-Ar), 8.15 (s, 1H, H-triazole), 8.14 (d, 2H, H-Ar), 8.03 (d, 2H, H-Ar), 7.54 (d, 2H, H-Ar), 7.32 (t,

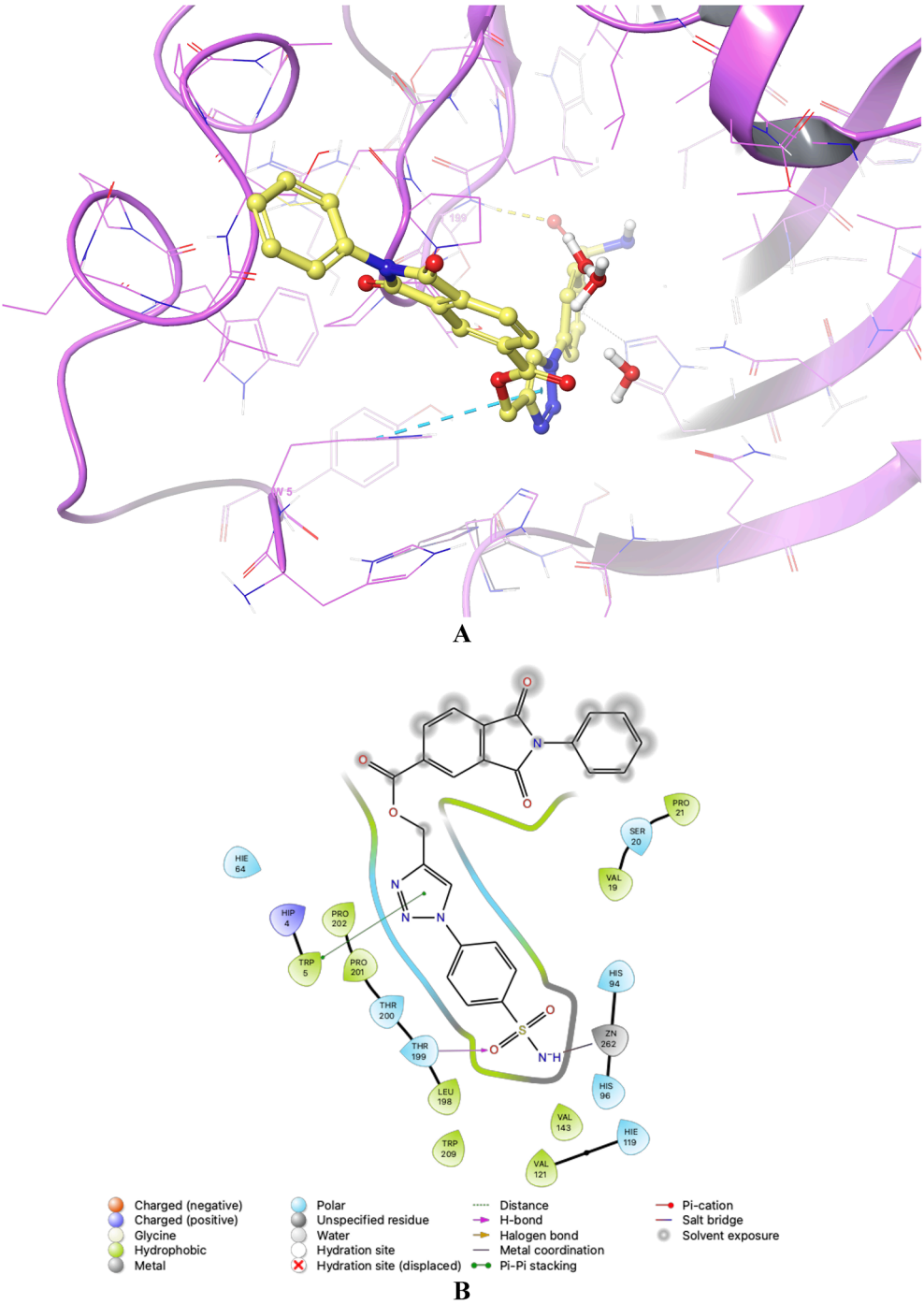

Figure 4. Molecular docking of *h*CA IX isoform (PDB ID 3IAI) with [1-(4-sulfamoylphenyl)-1*H*-1,2,3-triazol-4-yl]methyl 1,3-dioxo-2-phenylisoindoline-5-carboxylate (**7a**). **(A)** 3D docking pose of analogue **7a** within the binding pocket of 3IAI. In the 3D panel, hydrogen bonds and pi-pi stacking interactions are shown in yellow and blue dashed lines, respectively. Only the interacting amino acids are demonstrated for the sake of clarity. **(B)** 2D interaction diagram of 3IAI with analogue **7a**. (For interpretation of the references to colour in this figure legend, the reader is referred to the web version of this article.)

1H, H-Ar), 7.24 (s, 2H, –NH_2), 5.61 (s, 2H, –CH_2), 2.22 (s, 6H, –CH_3). ^{13}C NMR (75 MHz, DMSO-d_6) δ (ppm): 166.52, 164.68, 144.66, 143.77,139.17, 137.31, 136.63, 135,74, 135.67, 132.50, 130.29, 130.12, 129.03, 128.20, 125.14, 124.61, 124.17, 121.19, 59.35, 18.22. IR (ν, cm^{-1}: 3266 (NH_2), 3071 (=C—H), 1779 (C═O), 1100 (C—O), 1355 and 1163 (SO_2). QTOF LC-MS (m/zfound: (M−H): 530.1123; calculated [$C_{26}H_{21}N_5O_6S$]: 531.5415 [M]$^-$.

4.1.4.5. ***[1-(4-Sulfamoylphenyl)-1H-1,2,3-triazol-4-yl]methyl 2-(3-fluorophenyl)-1,3-dioxoisoindoline-5-carboxylate (7e)***. Beige solid, yield 68 %, m.p. 207 °C; ^{1}H NMR (300 MHz, DMSO-d_6) δ (ppm): 9.16 (s, 1H, H-Ar), 8.51 (d, 1H, H-Ar), 8.37 (d, 1H, H-Ar), 8.17 (s, 1H, H- triazole), 8.12 (d, 2H, H-Ar), 8.07 (d, 2H, H-Ar), 8.02 (s, 1H, H-Ar), 7.62–7.30 (m, 7H, H-Ar, –NH_2) 5.63 (s, 2H, –CH_2). ^{13}C NMR (75 MHz, DMSO-d_6) δ (ppm): 166.52, 164.70, 144.63, 143.69, 139.15, 136.42, 135.94, 135.45, 132.67, 131.30, 131.18, 128.22, 124.79, 124.25, 124.21, 124.12, 121.17, 115.26, 114.94, 59.29. IR (ν, cm^{-1}: 3235 (NH_2), 3061 (=C—H), 1776 (C═O), 1097 (C—O), 1348 and 1159 (SO_2). QTOF LC-MS (m/zfound: (M−H): 520.0715; calculated [$C_{24}H_{16}FN_5O_6S$]: 521.4835 [M]$^-$.

4.1.4.6. [1-(4-Sulfamoylphenyl)-1H-1,2,3-triazol-4-yl]methyl 2-(2-iodophenyl)-1,3-dioxoisoindoline-5-carboxylate (7f). White solid, yield 31 %, m.p. 191 °C; ^{1}H NMR (300 MHz, DMSO-d_6) δ (ppm): 9.12 (s, 1H, H-Ar), 8.50 (d, 1H, H-Ar), 8.42 (d, 1H, H-Ar), 8.19 (s, 1H, H-triazole), 8.14 (d, 2H, H-Ar), 8.03 (d, 2H, H-Ar), 7.99 (d, 1H, H-Ar), 7.56–7.40 (m, 4H, H-

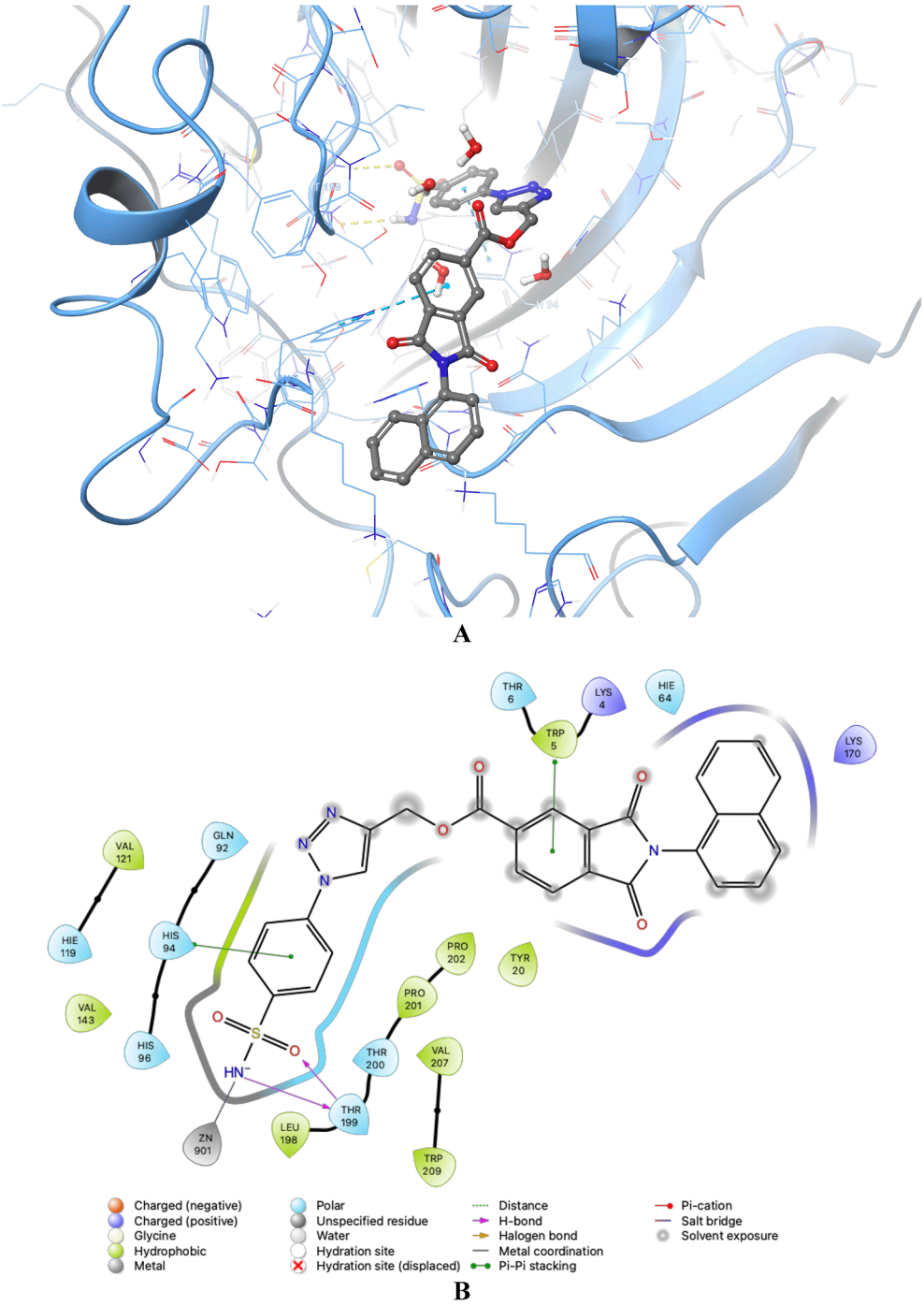

Figure 5. Molecular docking of *h*CA XII isoform (PDB ID 1JD0) with [1-(4-sulfamoylphenyl)-1*H*-1,2,3-triazol-4-yl]methyl 2-(naphthalen-1-yl)-1,3-dioxoisoindoline-5-carboxylate (**7h**). **(A)** 3D docking pose of analogue **7h** within the binding pocket of 1JD0. In the 3D panel, hydrogen bonds and pi-pi stacking interactions are shown in yellow and blue dashed lines, respectively. Only the interacting amino acids are demonstrated for the sake of clarity. **(B)** 2D interaction diagram of 1JD0 with analogue **7h**. (For interpretation of the references to colour in this figure legend, the reader is referred to the web version of this article.)

Ar, $-NH_2$), 7.25 (m, 1H, H-Ar), 5.61 (s, 2H, $-CH_2$). ^{13}C NMR (75 MHz, DMSO-d_6) δ (ppm): 166.17, 164.63, 144.62, 139.80, 139.18, 136.76, 135.86, 135.79, 135.55, 132.60, 132.17, 131.30, 130.14, 128.22, 125.10, 124.55, 124.17, 121.20, 100.86, 59.38. IR (ν, cm^{-1}: 3264 (NH_2), 3077 (=C—H), 1781 (C=O), 1098 (C—O), 1350 and 1161 (SO_2). QTOF LC-MS (m/zfound: (M−H): 628.9612; calculated [$C_{24}H_{16}IN_5O_6S$]: 629.3912 [M]$^-$.

4.1.4.7. ***[1-(4-Sulfamoylphenyl)-1H-1,2,3-triazol-4-yl]methyl 2-(4-cyanophenyl)-1,3-dioxoisoindoline-5-carboxylate (7g)***. Brown solid, yield 60 %, m.p. 179 °C; ^{1}H NMR (300 MHz, DMSO-d_6) δ (ppm): 9.11 (s, 1H. H-Ar), 8.47 (d, 1H, H-Ar), 8.35 (d, 1H, H-Ar), 8.16 (s, 1H, H- triazole), 8.13 (d, 2H, H-Ar), 8.04 (d, 2H, H-Ar), 7.71 (d, 2H, H-Ar), 7.68 (d, 2H, H-Ar), 7.55 (s, 2H, $-NH_2$), 5.59 (s, 2H, $-CH_2$). ^{13}C NMR (75 MHz, DMSO-d_6) δ (ppm): 166.27, 164.65, 144.64, 143.71, 139.17, 136.56, 136.49, 135.91, 135.56, 133.72, 132.67, 128.31, 128.21, 124.87, 124.31, 121.17, 119,08, 11.24, 59.34. IR (ν, cm^{-1}: 3315 (NH_2), 3077 (=C—H), 1779 (C=O), 1091 (C—O), 1345 and 1151 (SO_2). QTOF LC-MS (m/zfound: (M−H): 527.0761; calculated [$C_{25}H_{16}N_6O_6S$]: 528.5043 [M]$^-$.

4.1.4.8. [1-(4-Sulfamoylphenyl)-1H-1,2,3-triazol-4-yl]methyl 2-(naphthalen-1-yl)-1,3-dioxoisoindoline-5-carboxylate (7h). Pink solid, yield 35 %, m.p. 185 °C; ^{1}H NMR (300 MHz, DMSO-d_6) δ (ppm): 9.16 (s, 1H, H-Ar), 8.55 (d, 1H, H-Ar), 8.43 (s, 1H, H-Ar), 8.20 (s, 1H, H-triazole), 8.17 (d, 1H, H-Ar), 8.10 (d, 1H, H-Ar), 8.06 (d, 1H, H-Ar), 7.91 (d, 1H, H-Ar),

Table 4
ADME-Tox related parameters[a] of novel synthesized 1,2,3-triazole based benzenesulfonamides **7a-l** and the reference inhibitor acetazolamide, a clinically used drug.

Compounds ID	MW	Dipole	Volume	QPlogPoct	QPlogPw	QPlogPo/w	QPlogKp	QPlogKhsa	PSA	Rule of Five	Rule of Three	PAINS
7a	503.49	2.88	1457.50	28.10	20.26	1.68	–5.65	0.37	193.28	2	2	0
7b	537.93	4.36	1498.92	28.87	20.08	2.16	–5.61	0.14	192.37	2	2	0
7c	537.93	4.82	1501.00	28.94	20.02	2.15	–5.81	0.14	193.22	2	2	0
7d	531.54	4.28	1554.48	29.10	19.74	2.35	–5.47	0.28	188.57	2	2	0
7e	521.48	8.65	1475.17	29.00	20.06	1.91	–5.79	0.78	193.19	2	2	0
7f	629.39	4.88	1518.30	29.22	20.09	2.31	–5.63	0.19	193.57	2	2	0
7 g	528.50	7.94	1527.24	30.27	21.89	0.93	–7.00	–0.14	219.74	2	2	0
7 h	553.55	4.27	1594.42	30.39	20.85	2.63	–5.28	0.37	192.77	2	2	0
7i	561.53	5.03	1546.05	29.44	20.81	1.57	–5.59	–0.11	213.43	2	2	0
7j	539.61	7.49	1706.32	29.08	17.81	2.92	–5.72	0.34	195.18	2	2	0
7 k	511.55	2.28	1584.84	27.56	18.09	2.19	–5.91	0.13	195.18	2	2	0
7 l	483.50	8.40	1462.22	27.04	18.36	1.46	–6.07	–0.83	195.11	1	2	0
AAZ[b]	222.24	10.76	634.43	17.57	15.15	–1.75	–5.90	–0.97	134.97	0	0	0

[a] Various computational pharmacodynamic and pharmacokinetic parameters of synthesized compounds in this research were predicted such as molecular weight of the compound (MW; 130.00–725.00), computed dipole moment of the compound (Dipole; 1.00–12.50), total solvent-accessible volume in cubic angstroms using a probe with a 1.4 Å Radius (Volume; 500.00–2000.00), octanol/gas partition coefficient (QPlogPoct; 8.00–35.00), water/gas partition coefficient (QPlogPw; 4.00–45.00), octanol/water partition coefficient (QPlogPo/w; –2.00–6.50), skin permeability (QPlogKp; –8.00 - –1.00), prediction of binding to human serum albumin (QPlogKhsa; –1.50–1.50), van der Waals surface area of polar nitrogen and oxygen atoms (PSA; 7.00–200.00), number of violations of Lipinski's rule of five (max. 4), number of violations of Jorgensen's rule of three (max. 3), and pan-assay interference compounds (PAINS) alert.
[b] Acetazolamide.

7.85 (d, 2H, H-Ar), 7,82–7.56 (m, 7H, H-Ar, –NH_2), 5.65 (s, 2H, –CH_2). ^{13}C NMR (75 MHz, DMSO-d_6) δ (ppm): 167.50, 164.82, 144.65, 143.75, 139.18, 136.46, 136.32, 1355.38, 134.41, 133.18, 130.73, 130.33, 128.97, 128.21, 128.08, 127.84, 127.35, 126.32, 124.86, 124.31, 124.24, 123.63, 121.21, 59.32. IR (ν, cm^{-1}: 3363 (NH_2), 3045 (=C—H), 1779 (C═O), 1099 (C—O), 1349 and 1162 (SO_2). QTOF LC-MS (m/zfound: (M−H): 553.0812; calculated [$C_{28}H_{19}N_5O_6S$]: 553.5517 [M]$^-$.

*4.1.4.9. **[1-(4-Sulfamoylphenyl)-1H-1,2,3-triazol-4-yl]methyl 2-(benzo[d]dioxol-5-ylmethyl)-1,3-dioxoisoindoline-5-carboxylate (7i)**.* Beige solid, yield 87 %, m.p. 210 °C; ^{1}H NMR (300 MHz, DMSO-d_6) δ (ppm): 9.09 (s, 1H, H-Ar), 8.39 (d, 1H, H-Ar), 8.25–8.00 (m, 7H, H-Ar), 7.55 (s, 2H, –NH_2), 6.85 (d, 1H, H-Ar), 6.80 (s, 1H, H-Ar), 5.94 (s, 2H, –CH_2), 5.58 (s, 2H, –CH_2). ^{13}C NMR (75 MHz, DMSO-d_6) δ (ppm): 167.50, 164.71, 148.03, 147.27, 144.63, 143.72, 139.16, 136.16, 136.06, 135.18, 132.78, 130.74, 128.0, 124.40, 124.18, 123.93, 121.76, 121.15, 108.80, 101.71, 59.23. IR (ν, cm^{-1}: 3265 (NH_2), 3074 (=C—H), 1777 (C═O), 1094 (C—O), 1355 and 1160 (SO_2). QTOF LC-MS (m/zfound: (M−H): 560.0863; calculated [$C_{26}H_{19}N_5O_8S$]: 561.5372 [M]$^-$.

4.1.4.10. [1-(4-Sulfamoylphenyl)-1H-1,2,3-triazol-4-yl]methyl 2-octyl-1,3-dioxoisoindoline-5-carboxylate (7j). White solid, yield 47 %, m.p. 181 °C; ^{1}H NMR (300 MHz, DMSO-d_6) δ (ppm): 9.11 (s, 1H, H-Ar), 8.38 (d, 1H, H-Ar), 8.24 (d, 1H, H-Ar), 8.17 (s, 1H, H-triazole), 8.14 (d, 2H, H-Ar), 8.03 (d, 2H, H-Ar), 7.55 (s, 2H, –NH_2), 5.58 (s, 2H, –CH_2), 3.55 (t, 2H, –CH_2), 1.56 (quin, 2H, –CH_2), 1.20 (m, 10*H*, –CH_2),), 0.83 (t, 3H, –CH_3), ^{13}C NMR (75 MHz, DMSO-d_6) δ (ppm): 167.69, 164.69, 144.62, 143.70,139.15, 136.06, 135.05, 132.77, 128.19, 128.18, 123.67, 121.09, 59.20, 40.96, 31.87, 29.23, 29.19, 28.47, 26.91, 22.74, 14.58. IR (ν, cm^{-1}: 3340 (NH_2), 3156 (=C—H), 2923 (–CH), 1771 (C═O), 1706 (C═O), 1089 (C—O), 1347 and 1162 (SO_2). QTOF LC-MS (m/zfound: (M−H): 538.1748; calculated [$C_{26}H_{29}N_5O_6S$]: 539.6124 [M]$^-$.

4.1.4.11. [1-(4-Sulfamoylphenyl)-1H-1,2,3-triazol-4-yl]methyl 2-hexyl-1,3-dioxoisoindoline-5-carboxylate (7k). Orange solid, yield 40 %, m.p. 194 °C; ^{1}H NMR (300 MHz, DMSO-d_6) δ (ppm): 9.08 (s, 1H, H-Ar), 8.37 (d, 1H, H-Ar), 8.20 (d, 1H, H-Ar), 8.12 (s, 1H, H-triazole), 8.03 (d, 2H, H-Ar), 7.94 (d, 2H, H-Ar), 7.54 (s, 2H, –NH_2), 5.56 (s, 2H, –CH_2), 3.53 (t, 2H, –CH_2), 1.54 (quin, 2H, –CH_2), 1.21 (m, 6H, –CH_2), 0.79 (t, 3H, –CH_3). ^{13}C NMR (75 MHz, DMSO-d_6) δ (ppm): 167.69, 164.70, 144.64, 143.71, 139.15, 136.05, 135.07, 132.76, 128.20, 124.17, 124.13, 123.68, 121.11, 59.21, 40.97, 31.42, 28.43, 26.56, 22.61, 14.51. IR (ν, cm^{-1}: 3366 (NH_2), 3265 (=C—H), 2927 (–CH), 1770 (C═O), 1102 (C—O), 1350 and 1152 (SO_2). QTOF LC-MS (m/zfound: (M−H): 510.1437; calculated [$C_{24}H_{25}N_5O_6S$]: 511.5526 [M]$^-$.

*4.1.4.12. **[1-(4-Sulfamoylphenyl)-1H-1,2,3-triazol-4-yl]methyl 2-butyl-1,3-dioxoisoindoline-5-carboxylate (7l)**.* Beige solid, yield 74 %, m.p. 213 °C; ^{1}H NMR (300 MHz, DMSO-d_6) δ (ppm): 9.09 (s, 1H, H-Ar), 8.36 (d, 1H, H-Ar), 8.13 (s, 1H, H-triazole), 8.03 (d, 2H, H-Ar), 8.01 (d, 2H, H-Ar), 7.90 (t, 1H, H-Ar), 7.55 (s, 2H, –NH_2), 5.57 (s, 2H,–CH_2), 3.55 (t, 2H, –CH_2), 1.53 (quin, 2H, –CH_2), 1.27 (sextet, 2H, –CH_2), 0.86 (t, 3H, –CH_3). ^{13}C NMR (75 MHz, DMSO-d_6) δ (ppm): 167.75, 164.73, 144.63, 143.72, 139.10, 136.10, 136, 135, 132.81, 128.20, 124.20, 123.68, 121.15, 59.22, 39.29, 30.57, 20.16, 14.16. IR (ν, cm^{-1}: 3334 (NH_2), 3256 (=C—H), 2963 (–CH), 1773 (C═O), 1094 (C—O), 1340 and 1160 (SO_2). QTOF LC-MS (m/zfound: (M−H): 482.1122; calculated [$C_{22}H_{21}N_5O_6S$]: 483.5064 [M]$^-$.

4.2. Carbonic anhydrase inhibitory effect study

The esterase activity of the *h*CAs, *h*CA I, II, IV, IX, and XII isoforms were tested using Verpoorte's method[56] of detecting the change in absorbance at 348 nm to determine the inhibitory effects of novel produced 1,3-dioxoisoindolin-5-carboxylate analogues **7a-l**.[57–59] These analogues (**7a-l**) and AAZ were dissolved in DMSO at an initial concentration of 1 mg/ml. Around 1 % of DMSO was present in the final reaction mixture. As in past research, the substrate 4-nitrophenyl acetate (PubChem CID: 13243) was used to assess the activity of *h*CA isoforms.[60–62] The amount of enzyme necessary to release mol of product per minute at 25 °C was defined as one enzyme unit. Three measurements were made on each sample. To investigate the *in vitro* inhibitory mechanisms of the analogues (**7a-l**), kinetic assays were done with various substrate and chemical concentrations.[63–65] The observed data were used to produce IC_{50} plots, Michaelis-Menten curves, and Lineweaver-Burk plots and to determine K_I constants and different types of inhibition.

4.3. Antiproliferative activity study

For *in vitro* anticancer activity against the A549 cell line (CCL-185™), 1,3-dioxoisoindolin-5-carboxylate analogues (**7a-l**) were evaluated using an MTT assay.[66] A549 cells were seeded into 96-well

microplates (5x10^3 cells/well). After overnight incubation at 37 °C, the analogues (**7a-l**) were added in increasing concentrations (10, 20, 40, 80, 120, and 160 μM; the compounds dissolved in DMSO, and the final DMSO concentration in the dilutions was less than 0.1 %). After 24 h of exposure, 50 μL of MTT solution was added to a final concentration of 0.5 mg/ml, and the cells were incubated at 37 °C for 4 h. The medium was aspirated, and formazan crystals were dissolved in DMSO (100 μL). After the contents dissolved, the wells' optical density was measured at 570 nm by a microplate spectrophotometer (Epoch™ spectrophotometer, BioTek Instruments, Inc., Vermont, USA). The viability of cells was determined by comparing formazan concentrations of the treated cells with those of untreated control cells. The values were means from three independent experiments (three wells each).

4.4. In silico study

Small-Molecule Drug Discovery Suite 2022–3 for Mac, the most recent version, was used for the molecular docking investigation (Schrödinger, LLC, NY, USA). The PDB IDs 1AZM (for *h*CA I, A chain, 2.00 Å),[67] 3HS4 (for *h*CA II, A chain, 1.10 Å),[68] 5JN8 (for *h*CA IV, A chain, 1.85 Å),[69] 3IAI (for *h*CA IX, B chain, 2.20 Å),[70] and 1JD0 (for *h*CA XII, A chain, 1.50 Å)[71] for the *h*CA isoforms used as the model for the experiment were taken from the RCSB Protein Data Bank (https://www.rcsb.org). The Protein Preparation Wizard workflow of the suite was used to prepare the protein structures to dock.[72] The structures of the 1,3-dioxoisoindolin-5-carboxylate analogues (**7a-l**) were built using ChemDraw software V21 for Mac (PerkinElmer, Inc., Waltham, MA, USA). These benzenesulfonamides **7a–l** were optimized with Epik[73] in the optimal potential liquid simulations 4 (OPLS4) force field using the LigPrep module,[74] a component of the same software package, at pH 7.4 ± 0.5. The active site residues identified by the SiteMap tool[75] were defined in the Receptor Grid Generation module to create the receptor grid in the Maestro panel.[76] To dock ligands to *h*CA isoforms with the default parameters, the extra precision (XP) approach of the Glide application was used.[77–80] Additionally, it has been determined how well the MM-GBSA predicts relative binding affinity in the VSGB energy model[81–84] and OPLS4 force field using the ligand complexes 1AZM, 3HS4, 5JN8, 3IAI, and 1JD0.

4.5. Statistical study

Analysis of the data and drawing of graphs were realized using GraphPad Prism V9 for Mac (GraphPad Software, La Jolla California USA). The inhibition constants were calculated by SigmaPlot V12 for Windows (Systat Software, San Jose California USA). The fit of enzyme inhibition models was compared using the extra sum-of-squares F test and the AICc approach. The results were exhibited as mean ± standard error of the mean (95 % confidence intervals). Differences between data sets were considered statistically significant when the *p*-value was less than 0.05.

Data availability.

Data will be made available on request.

Declaration of Competing Interest

The authors declare that they have no known competing financial interests or personal relationships that could have appeared to influence the work reported in this paper.

Data availability

Data will be made available on request.

Acknowledgements

This work was supported by the Research Fund of Sakarya University (grant number 2021-7-24-56), the Research Fund of Erzincan Binali Yıldırım University (grant number TSA-2020-729), and the Research Fund of Anadolu University (grant number 2102S003).

Appendix A. Supplementary material

Supplementary data to this article can be found online at https://doi.org/10.1016/j.bmc.2022.117111.

References

1 Eftekhari-Sis B, Zirak M. Chemistry of α-Oxoesters: A Powerful Tool for the Synthesis of Heterocycles. *Chem Rev*. 2015;115:151–264. https://doi.org/10.1021/cr5004216.
2 I.A. Carbajal-Valenzuela, N.M. Apolonio–Hernandez, D.V. Gutierrez-Chavez, B. González-Arias, A. Jimenez-Hernandez, I. torres-Pacheco, E. Rico-García, A.A. Feregrino-Pérez, R.G. Guevara-González, Chapter 5 - Biological macromolecules as nutraceuticals, in: A.K. Nayak, A.K. Dhara, D. Pal (Eds.) Biological Macromolecules, Academic Press2022, pp. 97-138.
3 De S, Aamna B, Sahu R, Parida S, Behera SK, Dan AK. Seeking heterocyclic scaffolds as antivirals against dengue virus. *Eur J Med Chem*. 2022;240, 114576. https://doi.org/10.1016/j.ejmech.2022.114576.
4 Alanzy AL, Bakhotm DA, Abdel-Rahman RM. Design, Synthesis, Chemistry and Biological Evaluation of Some Polyfunctional Heterocyclic Nitrogen Systems—Overview. *Int J Org Chem*. 2020;10:39. https://doi.org/10.4236/ijoc.2020.102003.
5 Hou W, Xu H. Incorporating Selenium into Heterocycles and Natural Products—From Chemical Properties to Pharmacological Activities. *J Med Chem*. 2022;65:4436–4456. https://doi.org/10.1021/acs.jmedchem.1c01859.
6 Obaid RJ, Mughal EU, Naeem N, et al. Pharmacological significance of nitrogen-containing five and six-membered heterocyclic scaffolds as potent cholinesterase inhibitors for drug discovery. *Process Biochem*. 2022;120:250–259. https://doi.org/10.1016/j.procbio.2022.06.009.
7 Kallander LS, Lu Q, Chen W, et al. 4-Aryl-1,2,3-triazole: A Novel Template for a Reversible Methionine Aminopeptidase 2 Inhibitor, Optimized To Inhibit Angiogenesis in Vivo. *J Med Chem*. 2005;48:5644–5647. https://doi.org/10.1021/jm050408c.
8 Aromí G, Barrios LA, Roubeau O, Gamez P. Triazoles and tetrazoles: Prime ligands to generate remarkable coordination materials. *Coord Chem Rev*. 2011;255:485–546. https://doi.org/10.1016/j.ccr.2010.10.038.
9 Bitla S, Gayatri AA, Puchakayala MR, et al. Design and synthesis, biological evaluation of bis-(1,2,3- and 1,2,4)-triazole derivatives as potential antimicrobial and antifungal agents. *Bioorg Med Chem Lett*. 2021;41, 128004. https://doi.org/10.1016/j.bmcl.2021.128004.
10 Bonandi E, Christodoulou MS, Fumagalli G, Perdicchia D, Rastelli G, Passarella D. The 1,2,3-triazole ring as a bioisostere in medicinal chemistry. *Drug Disc. T*. 2017;22:1572–1581. https://doi.org/10.1016/j.drudis.2017.05.014.
11 Ge X, Xu Z. 1,2,4-Triazole hybrids with potential antibacterial activity against methicillin-resistant Staphylococcus aureus. *Arch Pharm*. 2021;354:2000223. https://doi.org/10.1002/ardp.202000223.
12 Rahman MT, Decker AM, Laudermilk L, et al. Evaluation of Amide Bioisosteres Leading to 1,2,3-Triazole Containing Compounds as GPR88 Agonists: Design, Synthesis, and Structure-Activity Relationship Studies. *J Med Chem*. 2021;64:12397–12413. https://doi.org/10.1021/acs.jmedchem.1c01075.
13 Fang D, Zhang Z-Y, Shangguan Z, He Y, Yu C, Li T. (Hetero)arylazo-1,2,3-triazoles: "Clicked" Photoswitches for Versatile Functionalization and Electronic Decoupling. *J Am Chem Soc*. 2021;143:14502–14510. https://doi.org/10.1021/jacs.1c08704.
14 Dequina HJ, Eshon J, Schmid SC, et al. Re-Evaluation of Product Outcomes in the Rh-Catalyzed Ring Expansion of Aziridines with N-Sulfonyl-1,2,3-Triazoles. *J Org Chem*. 2022;87:10902–10907. https://doi.org/10.1021/acs.joc.2c01186.
15 Lallemang M, Yu L, Cai W, et al. Multivalent non-covalent interactions lead to strongest polymer adhesion. *Nanoscale*. 2022;14:3768–3776. https://doi.org/10.1039/D1NR08338D.
16 L. Cicco, F.M. Perna, A. Falcicchio, A. Altomare, F. Messa, A. Salomone, V. Capriati, P. Vitale, 1,3-Dipolar Cycloaddition of Alkanone Enolates with Azides in Deep Eutectic Solvents for the Metal-free Regioselective Synthesis of Densely Functionalized 1,2,3-Triazoles, Eur. J. Org. Chem., n/a. 10.1002/ejoc.202200843.
17 Mehrdadian M, Khazalpour S, Amani A. Electrochemical oxidation assisted with the 1,3-dipolar cycloaddition for the synthesis of the new substituted triazole. *J Electroanal Chem*. 2022;907, 116056. https://doi.org/10.1016/j.jelechem.2022.116056.
18 A. Oubella, A. Bimoussa, S. Byadi, M. Fawzi, Y. Laamari, A. Auhmani, H. Morjani, A. Robert, A. Riahi, M.Y. Ait Itto, Design, synthesis, in vitro anticancer activity, and molecular docking studies of new (R)-carvone-pyrazole-1,2,3-triazoles, J. Mol. Struct., 1265 (2022) 133383. 10.1016/j.molstruc.2022.133383.
19 Lauria A, Delisi R, Mingoia F, et al. 1,2,3-Triazole in Heterocyclic Compounds, Endowed with Biological Activity, through 1,3-Dipolar Cycloadditions. *Eur J Org Chem*. 2014;2014:3289–3306. https://doi.org/10.1002/ejoc.201301695.
20 Dheer D, Singh V, Shankar R. Medicinal attributes of 1,2,3-triazoles: Current developments. *Bioorg Chem*. 2017;71:30–54. https://doi.org/10.1016/j.bioorg.2017.01.010.
21 Xu Z, Song X-F, Hu Y-Q, Qiang M, Lv Z-S. Azide-alkyne cycloaddition towards 1H–1,2,3-triazole-tethered gatifloxacin and isatin conjugates: Design, synthesis and

in vitro anti-mycobacterial evaluation. *Eur J Med Chem.* 2017;138:66–71. https://doi.org/10.1016/j.ejmech.2017.05.057.
22 J. Akhtar, A.A. Khan, Z. Ali, R. Haider, M. Shahar Yar, Structure-activity relationship (SAR) study and design strategies of nitrogen-containing heterocyclic moieties for their anticancer activities, Eur. J. Med. Chem., 125 (2017) 143-189. 10.1016/j.ejmech.2016.09.023.
23 Fan Y-L, Cheng X-W, Wu J-B, et al. Antiplasmodial and antimalarial activities of quinolone derivatives: An overview. *Eur J Med Chem.* 2018;146:1–14. https://doi.org/10.1016/j.ejmech.2018.01.039.
24 Chu X-M, Wang C, Wang W-L, et al. Triazole derivatives and their antiplasmodial and antimalarial activities. *Eur J Med Chem.* 2019;166:206–223. https://doi.org/10.1016/j.ejmech.2019.01.047.
25 Xu Z, Zhao S-J, Liu Y. 1,2,3-Triazole-containing hybrids as potential anticancer agents: Current developments, action mechanisms and structure-activity relationships. *Eur J Med Chem.* 2019;183, 111700. https://doi.org/10.1016/j.ejmech.2019.111700.
26 Shi J, Ju R, Gao H, Huang Y, Guo L, Zhang D. Targeting glutamine utilization to block metabolic adaptation of tumor cells under the stress of carboxyamidotriazole-induced nutrients unavailability. *Acta Pharmacol. Sin. B.* 2022;12:759–773. https://doi.org/10.1016/j.apsb.2021.07.008.
27 Akocak S, Lolak N, Bua S, Nocentini A, Supuran CT. Activation of human α-carbonic anhydrase isoforms I, II, IV and VII with bis-histamine schiff bases and bis-spinaceamine substituted derivatives. *J Enzyme Inhib Med Chem.* 2019;34:1193–1198. https://doi.org/10.1080/14756366.2019.1630616.
28 C.T. Supuran, C. Capasso, Chapter 13 - Acatalytic Carbonic Anhydrases (CAs VIII, X, XI), in: C.T. Supuran, G. De Simone (Eds.) Carbonic Anhydrases as Biocatalysts, Elsevier, Amsterdam, 2015, pp. 239-245.
29 Alterio V, Di Fiore A, D'Ambrosio K, Supuran CT, De Simone G. Multiple Binding Modes of Inhibitors to Carbonic Anhydrases: How to Design Specific Drugs Targeting 15 Different Isoforms? *Chem Rev.* 2012;112:4421–4468. https://doi.org/10.1021/cr200176r.
30 Claudiu T. Supuran, Structure and function of carbonic anhydrases. *Biochem J.* 2016;473:2023–2032. https://doi.org/10.1042/bcj20160115.
31 Angeli A, Ferraroni M, Supuran CT. Famotidine, an Antiulcer Agent, Strongly Inhibits Helicobacter pylori and Human Carbonic Anhydrases. *ACS Med Chem Lett.* 2018;9:1035–1038. https://doi.org/10.1021/acsmedchemlett.8b00334.
32 Pacchiano F, Carta F, McDonald PC, et al. Ureido-Substituted Benzenesulfonamides Potently Inhibit Carbonic Anhydrase IX and Show Antimetastatic Activity in a Model of Breast Cancer Metastasis. *J Med Chem.* 2011;54:1896–1902. https://doi.org/10.1021/jm101541x.
33 Nocentini A, Bua S, Lomelino CL, et al. Discovery of New Sulfonamide Carbonic Anhydrase IX Inhibitors Incorporating Nitrogenous Bases. *ACS Med Chem Lett.* 2017;8:1314–1319. https://doi.org/10.1021/acsmedchemlett.7b00399.
34 A. Kumar, K. Siwach, T. Rom, R. Kumar, A. Angeli, A. Kumar Paul, C.T. Supuran, P.K. Sharma, Tail-approach based design and synthesis of Arylthiazolylhydrazono-1,2,3-triazoles incorporating sulfanilamide and metanilamide as human carbonic anhydrase I, II, IV and IX inhibitors, Bioorg. Chem., 123 (2022) 105764. 10.1016/j.bioorg.2022.105764.
35 Tars K, Vullo D, Kazaks A, et al. Sulfocoumarins (1,2-Benzoxathiine-2,2-dioxides): A Class of Potent and Isoform-Selective Inhibitors of Tumor-Associated Carbonic Anhydrases. *J Med Chem.* 2013;56:293–300. https://doi.org/10.1021/jm301625s.
36 Supuran CT. How many carbonic anhydrase inhibition mechanisms exist? *J Enzyme Inhib Med Chem.* 2016;31:345–360. https://doi.org/10.3109/14756366.2015.1122001.
37 Angeli A, Carta F, Nocentini A, et al. Carbonic Anhydrase Inhibitors Targeting Metabolism and Tumor Microenvironment. *Metabolites.* 2020;10:412.
38 Tanpure RP, Ren B, Peat TS, et al. Carbonic Anhydrase Inhibitors with Dual-Tail Moieties To Match the Hydrophobic and Hydrophilic Halves of the Carbonic Anhydrase Active Site. *J Med Chem.* 2015;58:1494–1501. https://doi.org/10.1021/jm501798g.
39 Supuran CT. Exploring the multiple binding modes of inhibitors to carbonic anhydrases for novel drug discovery. *Expert Opin. Drug Disc.* 2020;15:671–686. https://doi.org/10.1080/17460441.2020.1743676.
40 Bozdag M, Ferraroni M, Nuti E, et al. Combining the tail and the ring approaches for obtaining potent and isoform-selective carbonic anhydrase inhibitors: Solution and X-ray crystallographic studies. *Bioorg Med Chem.* 2014;22:334–340. https://doi.org/10.1016/j.bmc.2013.11.016.
41 Nocentini A, Supuran CT. Advances in the structural annotation of human carbonic anhydrases and impact on future drug discovery. *Expert Opin. Drug Disc.* 2019;14:1175–1197. https://doi.org/10.1080/17460441.2019.1651289.
42 Pinard MA, Mahon B, McKenna R. Probing the surface of human carbonic anhydrase for clues towards the design of isoform specific inhibitors. *Biomed Res Int.* 2015;2015. https://doi.org/10.1155/2015/453543.
43 Pala N, Micheletto L, Sechi M, et al. Carbonic Anhydrase Inhibition with Benzenesulfonamides and Tetrafluorobenzenesulfonamides Obtained via Click Chemistry. *ACS Med Chem Lett.* 2014;5:927–930. https://doi.org/10.1021/ml500196t.
44 Sharma V, Kumar R, Bua S, Supuran CT, Sharma PK. Synthesis of novel benzenesulfonamide bearing 1,2,3-triazole linked hydroxy-trifluoromethylpyrazolines and hydrazones as selective carbonic anhydrase isoforms IX and XII inhibitors. *Bioorg Chem.* 2019;85:198–208. https://doi.org/10.1016/j.bioorg.2019.01.002.
45 Salmon AJ, Williams ML, Wu QK, et al. Metallocene-Based Inhibitors of Cancer-Associated Carbonic Anhydrase Enzymes IX and XII. *J Med Chem.* 2012;55:5506–5517. https://doi.org/10.1021/jm300427m.
46 C.T. Supuran, V. Alterio, A. Di Fiore, K. D' Ambrosio, F. Carta, S.M. Monti, G. De Simone, Inhibition of carbonic anhydrase IX targets primary tumors, metastases, and cancer stem cells: Three for the price of one, Med. Res. Rev., 38 (2018) 1799-1836. 10.1002/med.21497.
47 Ebbesen P, Pettersen EO, Gorr TA, et al. Taking advantage of tumor cell adaptations to hypoxia for developing new tumor markers and treatment strategies. *J Enzyme Inhib Med Chem.* 2009;24:1–39. https://doi.org/10.1080/14756360902784425.
48 Waheed A, Sly WS. Carbonic anhydrase XII functions in health and disease. *Gene.* 2017;623:33–40. https://doi.org/10.1016/j.gene.2017.04.027.
49 Supuran CT. Carbonic anhydrase inhibitors as emerging agents for the treatment and imaging of hypoxic tumors. *Expert Opin Invest Drugs.* 2018;27:963–970. https://doi.org/10.1080/13543784.2018.1548608.
50 Baghban R, Roshangar L, Jahanban-Esfahlan R, et al. Tumor microenvironment complexity and therapeutic implications at a glance. *Cell Commun. Sign.* 2020;18:59. https://doi.org/10.1186/s12964-020-0530-4.
51 Becker HM. Carbonic anhydrase IX and acid transport in cancer. *Br J Cancer.* 2020;122:157–167. https://doi.org/10.1038/s41416-019-0642-z.
52 Lee S-H, Griffiths JR. How and Why Are Cancers Acidic? *Carbonic Anhydrase IX and the Homeostatic Control of Tumour Extracellular pH, Cancers.* 2020;12:1616. https://doi.org/10.3390/cancers12061616.
53 Lolak N, Akocak S, Durgun M, et al. Novel bis-ureido-substituted sulfaguanidines and sulfisoxazoles as carbonic anhydrase and acetylcholinesterase inhibitors. *Mol Divers.* 2022:1–15. https://doi.org/10.1007/s11030-022-10527-0.
54 Lipinski CA, Lombardo F, Dominy BW, Feeney PJ. Experimental and computational approaches to estimate solubility and permeability in drug discovery and development settings. *Adv Drug Deliv Rev.* 1997;23:3–25. https://doi.org/10.1016/S0169-409X(96)00423-1.
55 Duffy EM, Jorgensen WL. Prediction of Properties from Simulations: Free Energies of Solvation in Hexadecane, Octanol, and Water. *J Am Chem Soc.* 2000;122:2878–2888. https://doi.org/10.1021/ja993663t.
56 Verpoorte JA, Mehta S, Edsall JT. Esterase activities of human carbonic anhydrases B and C. *J Biol Chem.* 1967;242:4221–4229. https://doi.org/10.1016/S0021-9258(18)95800-X.
57 Istrefi Q, Türkeş C, Arslan M, et al. Sulfonamides incorporating ketene N, S-acetal bioisosteres as potent carbonic anhydrase and acetylcholinesterase inhibitors. *Arch Pharm.* 2020;353:e1900383.
58 Durgun M, Türkeş C, Işık M, et al. Synthesis, characterization, biological evaluation and in silico studies of sulfonamide Schiff bases. *J Enzyme Inhib Med Chem.* 2020;35:950–962. https://doi.org/10.1080/14756366.2020.1746784.
59 Güleç Ö, Türkeş C, Arslan M, et al. Cytotoxic effect, enzyme inhibition, and in silico studies of some novel N-substituted sulfonyl amides incorporating 1,3,4-oxadiazol structural motif. *Mol Divers.* 2022;26:2825–2845. https://doi.org/10.1007/s11030-022-10422-8.
60 Türkeş C, Arslan M, Demir Y, Cocaj L, Nixha AR, Beydemir Ş. Synthesis, biological evaluation and in silico studies of novel N-substituted phthalazine sulfonamide compounds as potent carbonic anhydrase and acetylcholinesterase inhibitors. *Bioorg Chem.* 2019;89, 103004. https://doi.org/10.1016/j.bioorg.2019.103004.
61 Lolak N, Akocak S, Türkeş C, et al. Synthesis, characterization, inhibition effects, and molecular docking studies as acetylcholinesterase, α-glycosidase, and carbonic anhydrase inhibitors of novel benzenesulfonamides incorporating 1,3,5-triazine structural motifs. *Bioorg Chem.* 2020;100, 103897. https://doi.org/10.1016/j.bioorg.2020.103897.
62 S. Askin, H. Tahtaci, C. Türkeş, Y. Demir, A. Ece, G.A. Çiftçi, Ş. Beydemir, Design, synthesis, characterization, in vitro and in silico evaluation of novel imidazo [2, 1-b] [1, 3, 4] thiadiazoles as highly potent acetylcholinesterase and non-classical carbonic anhydrase inhibitors, Bioorg. Chem., (2021) 105009. 10.1016/j.bioorg.2021.105009.
63 Gündoğdu S, Türkeş C, Arslan M, Demir Y, Beydemir Ş. New Isoindole-1, 3-dione Substituted Sulfonamides as Potent Inhibitors of Carbonic Anhydrase and Acetylcholinesterase: Design. *Synthesis, and Biological Evaluation, ChemistrySelect.* 2019;4:13347–13355. https://doi.org/10.1002/slct.201903458.
64 Işık M, Akocak S, Lolak N, et al. Synthesis, characterization, biological evaluation, and in silico studies of novel 1,3-diaryltriazene-substituted sulfathiazole derivatives. *Arch Pharm.* 2020;353:e2000102.
65 Kalaycı M, Türkeş C, Arslan M, Demir Y, Beydemir Ş. Novel benzoic acid derivatives: Synthesis and biological evaluation as multitarget acetylcholinesterase and carbonic anhydrase inhibitors. *Arch Pharm.* 2021;354:2000282. https://doi.org/10.1002/ardp.202000282.
66 Zhang S, Li T, Zhang Y, et al. A new brominated chalcone derivative suppresses the growth of gastric cancer cells in vitro and in vivo involving ROS mediated up-regulation of DR5 and 4 expression and apoptosis. *Toxicol Appl Pharmacol.* 2016;309:77–86. https://doi.org/10.1016/j.taap.2016.08.023.
67 Chakravarty S, Kannan KK. Drug-Protein Interactions: Refined Structures of Three Sulfonamide Drug Complexes of Human Carbonic Anhydrase I Enzyme. *J Mol Biol.* 1994;243:298–309. https://doi.org/10.1006/jmbi.1994.1655.
68 Sippel KH, Robbins AH, Domsic J, Genis C, Agbandje-McKenna M, McKenna R. High-resolution structure of human carbonic anhydrase II complexed with acetazolamide reveals insights into inhibitor drug design, Acta Crystallogr. *Sect. F.* 2009;65:992–995. https://doi.org/10.1107/S1744309109036665.
69 Mickevičiūtė A, Timm DD, Gedgaudas M, et al. Intrinsic thermodynamics of high affinity inhibitor binding to recombinant human carbonic anhydrase IV. *Eur Biophys J.* 2018;47:271–290. https://doi.org/10.1007/s00249-017-1256-0.
70 Alterio V, Hilvo M, Di Fiore A, et al. Crystal structure of the catalytic domain of the tumor-associated human carbonic anhydrase IX. *Proc Natl Acad Sci.* 2009;106:16233–16238. https://doi.org/10.1073/pnas.0908301106.

71 Whittington DA, Waheed A, Ulmasov B, et al. Crystal structure of the dimeric extracellular domain of human carbonic anhydrase XII, a bitopic membrane protein overexpressed in certain cancer tumor cells. *Proc Natl Acad Sci*. 2001;98:9545–9550. https://doi.org/10.1073/pnas.161301298.

72 Madhavi Sastry G, Adzhigirey M, Day T, Annabhimoju R, Sherman W. Protein and ligand preparation: parameters, protocols, and influence on virtual screening enrichments. *J Comput Aided Mol Des*. 2013;27:221–234. https://doi.org/10.1007/s10822-013-9644-8.

73 Shelley JC, Cholleti A, Frye LL, Greenwood JR, Timlin MR, Uchimaya M. Epik: a software program for pKaprediction and protonation state generation for drug-like molecules. *J Comput Aided Mol Des*. 2007;21:681–691. https://doi.org/10.1007/s10822-007-9133-z.

74 Türkeş C, Akocak S, Işık M, et al. Novel inhibitors with sulfamethazine backbone: Synthesis and biological study of multi-target cholinesterases and α-glucosidase inhibitors. *J Biomol Struct Dyn*. 2021:1–13. https://doi.org/10.1080/07391102.2021.1916599.

75 Halgren TA. Identifying and Characterizing Binding Sites and Assessing Druggability. *J Chem Inf Model*. 2009;49:377–389. https://doi.org/10.1021/ci800324m.

76 Türkeş C, Demir Y, Beydemir Ş. Calcium Channel Blockers: Molecular Docking and Inhibition Studies on Carbonic Anhydrase I and II Isoenzymes. *J Biomol Struct Dyn*. 2021;39:1672–1680. https://doi.org/10.1080/07391102.2020.1736631.

77 Friesner RA, Banks JL, Murphy RB, et al. A New Approach for Rapid, Accurate Docking and Scoring. 1. Method and Assessment of Docking Accuracy. *J Med Chem*. 2004;47:1739–1749. https://doi.org/10.1021/jm0306430.

78 Friesner RA, Murphy RB, Repasky MP, et al. Extra Precision Glide: Docking and Scoring Incorporating a Model of Hydrophobic Enclosure for Protein−Ligand Complexes. *J Med Chem*. 2006;49:6177–6196. https://doi.org/10.1021/jm051256o.

79 Kilic A, Beyazsakal L, Işık M, et al. Mannich reaction derived novel boron complexes with amine-bis(phenolate) ligands: synthesis, spectroscopy and in vitro/in silico biological studies. *J Organomet Chem*. 2020;927, 121542. https://doi.org/10.1016/j.jorganchem.2020.121542.

80 Osmaniye D, Türkeş C, Demir Y, Özkay Y, Beydemir Ş, Kaplancıklı ZA. Design, synthesis, and biological activity of novel dithiocarbamate-methylsulfonyl hybrides as carbonic anhydrase inhibitors. *Arch Pharm*. 2022;355:e2200132.

81 Barreiro G, Guimarães CRW, Tubert-Brohman I, Lyons TM, Tirado-Rives J, Jorgensen WL. Search for Non-Nucleoside Inhibitors of HIV-1 Reverse Transcriptase Using Chemical Similarity, Molecular Docking, and MM-GB/SA Scoring. *J Chem Inf Model*. 2007;47:2416–2428. https://doi.org/10.1021/ci700271z.

82 Sever B, Türkeş C, Altıntop MD, Demir Y, Beydemir Ş. Thiazolyl-pyrazoline derivatives: In vitro and in silico evaluation as potential acetylcholinesterase and carbonic anhydrase inhibitors. *Int J Biol Macromol*. 2020;163:1970–1988. https://doi.org/10.1016/j.ijbiomac.2020.09.043.

83 Sever B, Türkeş C, Altıntop MD, Demir Y, Çiftçi GA, Beydemir Ş. Novel metabolic enzyme inhibitors designed through the molecular hybridization of thiazole and pyrazoline scaffolds. *Arch Pharm*. 2021;354:e2100294.

84 Yaşar Ü, Gönül İ, Türkeş C, Demir Y, Beydemir Ş. Transition-metal complexes of bidentate schiff-base ligands: in vitro and in silico evaluation as non-classical carbonic anhydrase and potential acetylcholinesterase inhibitors. *ChemistrySelect*. 2021;29:7278–7284. https://doi.org/10.1002/slct.202102082.